PART V

ABSORPTIVE-MEDIATED ENDOCYTOSIS OF A DYNORPHIN-LIKE ANALGESIC PEPTIDE, E-2078, INTO THE BLOOD-BRAIN BARRIER

SUMMARY

The binding and internalization of a novel analogue of dynorphin-like analgesic basic peptide, CH_3-[^{125}I]Tyr-Gly-Gly-Phe-Leu-Arg-CH_3Arg-D-Leu-NHC_2H_5 ([^{125}I]E-2078), by isolated bovine brain capillaries were investigated. High-performance liquid chromatographic analysis showed that no significant metabolism of [^{125}I]E-2078 occurred during incubation with brain capillaries for 30 min at 37°C. The binding of [^{125}I]E-2078 to brain capillaries increased with time and the steady-state cell-to-medium concentration ratio was 58.5 $\pm$ 2.6 µl/mg protein. Approximately a fourth of the [^{125}I]E-2078 binding was resistant to acid wash, and showed significant dependence on temperature and medium osmolarity. The acid sensitive binding of [^{125}I]E-2078, which presumably represents surface binding, was saturable and the Scatchard plot gave a maximal binding capacity (B_{max}) = 147 $\pm$ 29 pmol/mg protein, and a half-saturation constant (K_D) = 4.62 $\pm$ 0.59 µM. Pretreatment of brain capillaries with phenylarsine oxide, an endocytosis inhibitor, completely suppressed the acid resistant binding of [^{125}I]E-2078, but did not influence the surface binding of [^{125}I]E-2078. The acid resistant binding of [^{125}I]E-2078 was inhibited by poly-L-lysine and protamine, but not inhibited by insulin, transferrin, dynorphin (1-8), β-neoendorphin, naloxone or poly-L-glutamate. Moreover, *in vivo* brain extraction of [^{125}I]E-2078 in rats was 368 $\pm$ 55 % higher than that of [^{3}H]sucrose and was significantly inhibited by 1 mM of unlabeled E-2078. These results demonstrate that E-2078 is internalized by brain capillaries *via* absorptive-mediated endocytosis, which is a polycation-sensitive pathway.

INTRODUCTION

Dynorphin (1-8) and dynorphin (1-13) are naturally occurring opioid peptides distributed in the central nervous system of vertebrates (1). The current evidence indicates that they may be involved in the regulation of synaptic transmission related to the κ-type opioid receptor (2). Similar to other opioid peptides such as β-endorphin (3) and enkephalins (4), dynorphin is very susceptible to enzymatic degradation (5). Despite the observation that these peptides have high affinity for opioid receptors (6), one cannot expect analgesic effect following systemic administration of these opioid peptide because of their instability to enzymatic degradation and very low permeability of the blood-brain barrier (BBB) (4).

A novel analogue of dynorphin (1-8), [N-methyl-Tyr^1, N-methyl-Arg^7, D-Leu^8]dynorphin(1-8)ethylamide (designated as E-2078), which has high affinity for the κ-type opioid receptor (7), is a newly developed synthetic peptide which was designed to be protected against various peptidases present in blood, peripheral tissues and brain to overcome the disadvantage that dynorphin(1-8) was readily degraded (8). Since analgesic activity of E-2078 has been found to be several times higher than that of morphine following systemic administration (7), this peptide is likely to cross the blood-brain barrier (BBB) and is thought to be a potential candidate as an analgesic neuro-pharmaceutical which can be effectively used in systemic administration. With regard to BBB transport of peptides, previous studies have reported the receptor-mediated transcytosis of peptides, e.g., insulin (9) and transferrin (10); the absorptive-mediated transcytosis of positively charged peptides, e.g., cationized albumin and β-endorphin-cationized albumin chimeric peptide (11); and the

saturable carrier-mediated transport of small peptides with an N-terminal tyrosine through the BBB (12). Accordingly, it is of great interest to investigate the transport mechanism of E-2078 across the BBB, because E-2078 (pI = 10.0) is a positively charged peptide at a physiological pH and also an octapeptide with an N-terminal tyrosine.

In order to clarify the possible mechanism of the BBB transport of a novel dynorphin-like peptide, E-2078, we examined whether a newly developed analgesic peptide, E-2078, can be bound and internalized by isolated brain capillaries as an *in vitro* model system of the BBB. Moreover, we performed *in vivo* brain uptake experiments in rats using the carotid artery injection technique (14) to validate the results from *in vitro* experiments, because the *in vivo* extraction of E-2078 across the brain may represent the binding of the peptide at the luminal (not abluminal) side of the endothelia of the brain capillaries.

MATERIALS AND METHODS

Animals. Male Wistar rats weighing 200-220 g were purchased from Sankyo Laboratory Co. (Toyama, Japan). They had free access to food and water.

Chemicals. The dynorphin-like analgesic peptide, [N-methyl Tyr^1, N-methyl Arg^7, D-Leu^8]dynorphin-A-(1-8)ethylamide (E-2078) and [^{125}I-Tyr]E-2078 with a specific activity of 0.82-21.4 mCi/mg were kindly supplied from Eisai Co., Ltd. (Tokyo, Japan). [^{3}H(G)-]Inulin (473 µCi/mg), L-[ring-2,6 ^{3}H(N)]phenylalanine (56.4 Ci/mmol), N-[1-^{14}C]butanol (1.1 mCi/ml), [^{14}C(U)]sucrose (4.6 mCi/mmol) and Protosol (tissue solubilizer) were purchased from New England Nuclear Corp. (Boston, MA). [^{125}I-Tyr^{A14}]Human insulin with a specific activity of approximately 2,000 Ci/mmol, and [6,6'(n-^{3}H)]sucrose (10.9 Ci/mmol) were purchased from Amersham International Ltd. (Buckinghamshire, UK). Clear-sol (liquid scintillation cocktail) was purchased from Nakarai Chemical Co. (Kyoto, Japan), and porcine dynorphin A (1-8) and β-neoendorphin from Peninsula Laboratories (Belmont, CA). Salmon roe protamine sulfate was obtained from Wako Pure Chemical Industries Ltd. (Osaka, Japan). Human holotransferrin was purchased from the Green Cross Corp. (Osaka, Japan). Ketaral 50 (ketamine hydrochloride) was purchased from Sankyo Co., Ltd. (Tokyo, Japan). Porcine insulin, naloxone hydrochloride, poly-L-lysine hydrobromide (MW 4,000), poly-L-glutamic acid sodium salt (MW 14,300), dextran (industrial grade, MW. 71,500), bovine serum albumin (Fraction V), xylazine and phenylarsine oxide were purchased from Sigma Chemical Co. (St. Louis, MO). The other chemicals were of reagent grade and were used without further purification.

Isolation of Bovine Brain Capillaries. Capillaries were prepared

from bovine brains with a mechanical homogenization technique (14). Bovine brains were graciously supplied, within 20 min after exanguination, from the Meat Inspection Center of Kanazawa City (Kanazawa, Japan) and immediately soaked in ice cold buffer B (103 mM NaCl, 4.7 mM KCl, 2.5 mM $CaCl_2$, 1.2 mM KH_2PO_4, 1.2mM $MgSO_4$, 15 mM N-2-hydroxy-ethylpiperazine-N'-2-ethanesulfonic acid (HEPES), pH 7.4). The cortex was scraped off from the brains and homogenized in buffer A composed of the above buffer B, which is containing additionally 25 mM $NaHCO_3$, 10 mM D-glucose, 1 mM pyruvic acid and 0.1 % bovine serum albumin in buffer B. An equal volume of 26 % dextran dissolved in buffer B was added to the brain homogenate and centrifuged for 10 min at 3,800 x g and at 4°C. The pellet was suspended with buffer A and passed over a 210 µm nylon mesh. The capillaries filtered through the mesh were suspended in buffer A and passed over a glass beads column (450 µm glass beads) to remove erythrocytes and nucleus. The glass beads with the adherent capillaries were transferred to a plastic beaker, kept settled, and the supernatant containing capillaries was decanted. The capillaries were resuspended in buffer C (0.02 mM 2-amino-2-hydroxymethyl-1,3-propanediol (Tris), 0.25 M sucrose, 2 mM DL-dithiothreitol) and stored at -70°C until use. Capillary protein was determined by the Lowry method (15) employing bovine serum albumin as a standard.

Bovine brain capillaries prepared in this laboratory had a transport activity of [^{3}H]L-phenylalanine and a specific binding activity of [^{125}I]insulin, which were very similar to those reported previously (16,17).

High-Performance Liquid Chromatographic (HPLC) Analysis. The extent

to which the capillary metabolized [^{125}I]E-2078 was determined by HPLC analysis. The mixture of [^{125}I]E-2078 (0.25 µCi/ml) and capillaries (600 µg protein) were incubated at 37°C for 30 min and centrifuged at 10,000 x g for 45 sec. The supernatant was deproteinized by mixing well with an equal volume of methanol and centrifuged at 15,000 rpm for 5 min. The resultant supernatant was loaded onto a reversed-phased HPLC column, µ-Bondapak C_{18} (30 cm x 3.9 mm i.d.; Waters Associates, Inc., Milford, MA.). The constant-flow solvent delivery system, LC-6A (Shimadzu Corp., Kyoto, Japan) was equipped with an ultraviolet detector, SPO-6A (Shimadzu Corp.) and a gradient programmer, SCL-6A (Shimadzu Corp.). A guard column, C_{18} CORASIL (Waters Associates, Inc.) was placed between the injector and the analytical column. The mobile phase consisted of 2 solvents, which are mixtures of water and acetonitrile, containing 0.065% (V/V) trifluoroacetic acid (TFA). Solvent A was 10% (V/V) acetonitrile and solvent B was 60% (V/V) acetonitrile. The loaded samples were eluted with a linear gradient of solvent B from 20 to 50% within 15 min, followed by a linear gradient of solvent B from 50 to 100% within next 5 min. The solvent flow rate was 1.5 ml/min. The column and solvents were kept at room temperature. The eluents were collected automatically and the radioactivity in each eluent (1 ml) was counted using a γ-counter, ARC-605 (Aloka Co., Ltd., Tokyo, Japan).

In Vitro Binding and Internalization Studies using Isolated Brain Capillaries. Binding of [^{125}I]E-2078 to isolated bovine brain capillaries was examined by a method similar to that reported previously (17). Brain capillaries (600 µg protein) was preincubated in 180 µl of the incubation buffer (pH 7.4, 141 mM NaCl, 4 mM KCl, 2.8 mM $CaCl_2$, 1 mM $MgSO_4$, 10 mM HEPES, 10mM D-glucose, 0.1% bovine

serum albumin, pH 7.4, 300 mOsm) at 37°C (or 4°C) for 5 min. A solution (20 µl) containing 0.05 µCi of [^{125}I]E-2078 and 2 µCi of [^{3}H]inulin was incubated with the capillary suspension in the absence and presence of various compounds, i.e., unlabeled E-2078, insulin, holotransferrin, dynorphin (1-8), β-neoendorphin, naloxone, poly-L-lysine, protamine, and poly-L-glutamate. At designated times after incubation, the mixture was centrifuged at 10,000 x g for 45 sec in a microcentrifuge MR-15A (Tomy Seiko Co., Ltd., Tokyo, Japan).

An acid-wash technique (14,18) was then employed to discriminate between the internalization and binding of [^{125}I]E-2078 to the capillary pellet. The pellet was resuspended in 400 µl of ice cold acetate-barbital buffer (0.028 M CH_3COONa, 0.12 M NaCl, 0.02 M barbital, pH 3.0) and placed on ice for 6 min, followed by centrifugation at 10,000 x g for 45 sec. The radioactivity in the supernatant (acid-soluble binding) was measured in a liquid scintillation counter, LSC-703 (Aloka Co. Ltd., Tokyo, Japan) and was supposed to represent surface binding of [^{125}I]E-2078. The radioactivity in the pellet (acid-resistant binding) was also measured after solubilization by 500 µl of 1 N-NaOH for 10 min at 60°C, and was supposed to represent internalized [^{125}I]E-2078. ^{3}H- and ^{125}I-radioactivities in each sample were separately measured as previously described (19).

Collapsed Capillary Study. In order to examine the effect medium-osmolarity on the internalization of [^{125}I]E-2078 by brain capillaries, a binding experiment was also carried out in a hypertonic buffer (the incubation buffer plus 1.0 M sucrose, 1,400 mOsm). The subsequent procedure was the same as described above.

Effect of Phenylarsine Oxide on the Internalization of [^{125}I]E-2078. Isolated brain capillaries were preincubated for 20 min at 37°C in the incubation buffer in the presence and absence of 10 μM phenylarsine oxide which is known as an endocytosis inhibitor (20,21). The acid resistant binding of [^{125}I]E-2078 was determined by the acid wash method as described above.

Data Calculation. The data on binding and internalization were expressed as the cell-to-medium concentration (cell/medium) ratio, corrected for an extracellular space using [^{3}H]inulin, which were calculated as follows:

For The Acid Resistant Binding:

Cell/Medium (μl/mg protein)

= [(^{125}I-R minus ^{125}I-S x ^{3}H-R/^{3}H-S)/mg capillary protein]

/[^{125}I-M/μl medium]

For the Total Binding:

Cell/Medium (μl/mg protein)

= [^{125}I-T/mg capillary protein]/[^{125}I-M/μl medium]

minus [^{3}H-T/mg protein]/[^{3}H-M/μl medium]

where ^{125}I-R and ^{125}I-S are the ^{125}I-radioactivity in the acid resistant and acid soluble fractions associated with brain capillaries, respectively; ^{3}H-R and ^{3}H-S are the ^{3}H-radioactivity in the acid resistant and acid soluble fractions associated with brain capillaries, respectively; ^{125}I-M and ^{3}H-M are ^{125}I- and ^{3}H-radioactivity per μl of incubation medium, respectively; and ^{125}I-T and ^{3}H-T represent ^{125}I-R plus ^{125}I-S and ^{3}H-R plus ^{3}H-S, respectively.

Moreover, the cell-to-medium concentration ratio of the acid soluble binding (surface binding) was determined as that of the total binding

minus that of the acid resistant binding.

In Vivo Brain Uptake Study. The uptake (or binding) of [^{125}I]E-2078 to the luminal side of rat brain capillaries was measured with the *in vivo* carotid injection technique (12). Two hundred μl of Ringer's-Hepes Buffer (141 mM NaCl, 4.0 mM KCl, 2.8 mM $CaCl_2$, 10 mM HEPES, pH 7.4) containing 5 μCi/ml of [^{125}I]E-2078 and 150 μCi/ml of [^{3}H]sucrose, an extracellular marker, was rapidly injected into the carotid artery in rats anesthetized with intramuscular doses of ketamine 235 mg/kg and xylazine 2.3 mg/kg. *In vivo* brain uptake study was also performed in the presence of either 5 mM of L-tyrosine or 1 mM of unlabeled E-2078 in the injectate. After 5 seconds, the rats were decapitated and the ipsilateral hemisphere to the injected side was dissected and solubilized in 3 ml of Protosol at 55°C for 3 hr. Then 0.6 ml of H_2O_2 was transferred to the sample tubes and, after standing at room temperature for 15 min, the samples were incubated at 55°C for 30 min. After neutralization with 128 μl of glacial acetic acid, the radioactivity in each sample was measured in a liquid scintillation counter. The percentage uptake (or binding) of [^{125}I]E-2078 into the brain, relative to the vascular space using [^{3}H]sucrose, was calculated as follows:

Percentage of [^{125}I]E-2078 uptake/[^{3}H]sucrose space

= [(^{125}I/^{3}H dpm) in brain]/[(^{125}I/^{3}H dpm) in injectate] x 100

RESULTS

Stability of [^{125}I]E-2078 in Brain Capillary Suspension. Figure 1 shows the HPLC chromatograms of [^{125}I]E-2078 in the capillary suspension before and after incubation at 37°C for 30 min. Obviously, no significant metabolism of the labeled peptide occurred, indicating that E-2078 is fairly stable against enzymatic degradation by the peptidases associated with brain capillaries.

Binding and Internalization of [^{125}I]E-2078 by Isolated Brain Capillaries. The acid resistant binding was measured to assess the internalization of [^{125}I]E-2078 into brain capillaries. Figure 2 illustrates the effect of acid washing period at 4°C with pH 3.0 acetate-barbital buffer on the total binding of [^{125}I]E-2078 to the brain capillaries. Release of acid sensitive binding of [^{125}I]E-2078 by mild acid wash was completed within 10 min, where 23.0 ± 0.7 % of the total binding of [^{125}I]E-2078 was supposed to be the internalized peptide and approximately 75% of the total binding was supposed to be the surface binding of the peptide to brain endothelial cells. In this study, therefore, 6 min was chosen as the time interval of acid washing, because it was enough to assess the internalization of the peptide by brain capillaries.

Time courses of the total and acid resistant bindings of [^{125}I]E-2078 to brain capillaries are illustrated in figure 3. The cell-to-medium concentration (cell/medium) ratio of total [^{125}I]E-2078 binding increased from 23.4 ± 6.2 to 61.1 ± 10.4 µl/mg protein during incubation for 30 min with brain capillaries at 37°C. Similarly, the cell/medium ratio of acid resistant [^{125}I]E-2078 binding was increased from 3.90 ± 0.67 to 19.1 ± 0.6 µl/mg protein during incubation for 30 min, while only a slight and time-independent acid resistant binding

of [^{3}H]inulin was observed for 30 min (1.01 ± 0.06 µl/mg protein). Additionally, acid resistant [^{125}I]E-2078 binding to capillaries was not inhibited by 5 mM L-tyrosine at 37°C for 30 min (data not shown), suggesting that E-2078 was bound and internalized, intact by the isolated brain capillaries.

The acid resistant binding of [^{125}I]E-2078 (0.4 µM) to brain capillaries was compared between 4°C and 37°C in figure 4. No significant time-dependency was observed for the acid resistant binding of [^{125}I]E-2078 at 4°C, while significant increase of the binding with time was observed at 37°C. At 4°C, the acid resistant binding after 30 min (2.93 ± 0.13 µl/mg protein) was low and almost the same as the initial, nonspecific acid-resistant zero time at 37°C (2.74 ± 0.48 µl/mg protein).

Effect of Medium Osmolarity on the Internalization of [^{125}I]E-2078. Figure 5 demonstrates that the acid resistant binding of [^{125}I]E-2078 at 37°C decreased significantly when the osmolarity was increased from 300 to 1,400 mOsm, and little internalization was observed when capillaries were collapsed by a high osmolarity of 1,400 mOsm. This finding suggests that [^{125}I]E-2078 was internalized into an osmotically reactive intracellular space.

Effect of Phenylarsine Oxide on the Internalization of [^{125}I]E-2078 As clearly shown in figure 6, phenylarsine oxide, an endocytosis inhibitor, almost completely inhibited the acid resistant binding of [^{125}I]E-2078. In contrast, phenylarsine oxide did not significantly change the surface binding of [^{125}I]E-2078 (data not shown).

Concentration Dependence of [^{125}I]E-2078 Binding and Internalization. Figure 7 shows the concentration dependence of the surface

binding of [^{125}I]E-2078 to brain capillaries at the equilibrium condition, indicating the saturable and non-saturable bindings. The Scatchard plot for saturable surface binding of [^{125}I]E-2078, where saturable surface binding was obtained from the surface binding minus non-saturable surface binding which was determined in the presence of 10 mM unlabeled E-2078, indicates an existence of monocomponent, saturable binding site of [^{125}I]E-2078 on the surface of the brain capillaries. The apparent binding capacity (B_{max}) was determined to be 147 $\pm$ 29 pmol/mg protein, and the half-saturation constant (K_D) to be 4.62 $\pm$ 0.59 μM.

Effects of Several Peptides and Opioids on the Total Binding and Internalization of [^{125}I]E-2078. As presented in figure 8, porcine insulin (10 μM), human holotransferrin (10 μM), porcine dynorphin (1-8) (1 mM), β-neoendorphin (1 mM) did not change the total and acid resistant bindings of [^{125}I]E-2078. In contrast, poly-L-lysine (300 μM) and protamine (300 μM), which are polycationic peptides, significantly inhibited both the total and acid resistant bindings of [^{125}I]E-2078, while polyglutamate (300 μM), a polyanionic peptide, did not. Naloxone, an opioid antagonist, significantly enhanced the total binding of [^{125}I]E-2078 to the capillaries, but did not change the acid resistant binding.

In Vivo Brain Uptake Study. Table 1 summarizes the results of *in vivo* brain uptake (or binding) of [^{125}I]E-2078 to the luminal side of brain capillaries in rats, determined by the carotid artery injection technique. The apparent brain uptake of [^{125}I]E-2078 was 3.7-fold higher than that of [^{3}H]sucrose which was used as an extracellular marker, and was significantly inhibited by a high concentration (1 mM) of unlabeled E-2078. No significant inhibition by 5 mM L-tyrosine

indicates that the apparent brain uptake was not result from the uptake of [^{125}I]tyrosine generated from peptidase digestion at the endothelium, but from the uptake and/or binding of the octapeptide, [^{125}I]E-2078, to the luminal side of brain capillaries.

DISCUSSION

In the transport studies of peptides using isolated brain capillaries, enzymatic degradation of peptides during incubation with brain capillaries could lead to a serious problem for assessing the specific binding and internalization (4). In the present study, a newly synthetized dynorphin-like peptide, E-2078, was found to be very stable to the peptidase associated with isolated brain capillaries (fig. 1), in contrast to endogenous opioid peptides such as dynorphin (5,8) and enkephalin (4). Moreover, no inhibition by 5 mM L-tyrosine of the acid resistant binding of [^{125}I]E-2078 to capillaries suggests that E-2078 could be bound and internalized as its intact form by isolated brain capillaries. These advantageous properties of E-2078 can be attributed to suitable chemical modifications of enzyme-susceptible sites of native dynorphin, i.e., N-methyl groups at N-terminal Tyr^{1} and at Arg^{7}, D-Leu^{8} instead of L-Leu^{8}, and an ethylamine group at C-terminal D-Leu^{8}.

Similar to the studies on the binding of insulin (17) and cationized albumin (11) to brain capillaries, the acid-wash procedure was effectively performed to dissociate the surface binding of E-2078 to brain capillaries. Using this procedure, we have demonstrated that the dynorphin-like basic octapeptide, E-2078, was specifically bound and internalized by isolated brain capillaries. Both extent of the total and acid resistant bindings of E-2078 at 37°C (fig. 3) were shown to be similar to those of [^{125}I-Tyr^{A14}]human insulin determined under the same conditions (data not shown), but significantly lower than those of cationized albumin reported previously (11). Moreover, the K_D value for the capillary surface binding of E-2078 (4.62 $\pm$ 0.59 μM) was shown to be 5.8-fold greater than that of cationized albumin

(0.8 $\pm$ 0.1 μM) (11), and 1000-fold greater than the K_D value for the receptor binding of E-2078 to brain synaptic membranes (4.6 nM) (unpublished data). Therefore, the specific binding site of E-2078 on the surface of brain capillaries might be different from the opioid receptors in terms of binding characteristics.

Significant temperature- and osmotic pressure-dependencies of acid resistant binding of [^{125}I]E-2078 (figs. 4 and 5) suggest that mild acid wash procedure could dissociate the surface binding of [^{125}I]E-2078 to brain capillaries and that E-2078 was significantly internalized by brain capillaries. The acid resistant binding of E-2078 with brain capillaries was completely inhibited by phenylarsine oxide (fig. 6), which is known to inhibit the internalization of epidermal growth factor (20) and insulin (21). Although a long time period of incubation with phenylarsine oxide seems to cause cytotoxicity to fibroblasts (21), the complete inhibitory effect of this reagent on the acid resistant binding of [^{125}I]E-2078 might not be attributed to its cytotoxic effect on the brain capillaries because of such a short period of pretreatment as 20 min.

In order to characterize the endocytosis system of [^{125}I]E-2078 into the brain capillaries, the inhibition studies were also carried out. Since the pI value of E-2078 is 10.0 (unpublished data), the peptide is positively charged at a physiological pH of 7.4. It is well known that the surface of endothelial cell membranes has negatively charged region (22). The remarkably different effects of polycations (i.e., poly-L-lysine and protamine) and a polyanion (i.e., poly-L-glutamate) on the total and acid resistant bindings of [^{125}I]E-2078 (fig. 8) strongly suggest that electrostatic interactions of [^{125}I]E-2078 with

the cell surface anionic sites play an important role in the surface binding and subsequent internalization of the peptide into the brain capillaries. Since similar inhibitory effects of polycations on the absorptive-mediated transcytosis of cationized-albumin through the BBB have been observed (11), E-2078 might be transported by an absorptive-mediated endocytosis system. This system is clearly discriminated from the receptor-mediated endocytosis with a high affinity which has been reported for some peptides, e.g., insulin (18), insulin-like growth factors (23) and transferrin (24). Dynorphin (1-8) and β-neoendorphin, which are the agonists of κ-type opioid receptor and also basic peptides, exhibited no inhibitory effects on the total and acid resistant bindings of [^{125}I]E-2078 (fig. 8), presumably due to rapid degradation of these opioid peptides at the surface of brain capillaries during incubation and/or some difference in a mechanism by which these peptides were bound by capillaries. The effect of naloxone, an opioid antagonist, on the acid resistant binding of [^{125}I]E-2078 (fig. 8) suggests that opioid receptors did not mediate the endocytosis of [^{125}I]E-2078 through the BBB. On the other hand, the significant influence of naloxone on the binding of [^{125}I]E-2078 to brain capillaries may suggest that E-2078 binding has an opioid component. However, the mechanism by which naloxone caused an increase, instead of a decrease, of the E-2078 binding is the object of much speculation at present. One possible explanation for this is that naloxone interacts allosterically with E-2078, which would result in the increase of affinity of the E-2078 binding to the putative binding site on the brain capillaries.

It has been proposed that the transcytosis of peptide is composed of at least three steps, e.g., 1) the binding and internalization at the

luminal side of endothelial cell membrane, 2) diffusion through the cytoplasm of endothelial cell, 3) the externalization at the abluminal side of endothelial cell membrane (25). It is hard to distinguish between the endocytosis systems present at the luminal side and abluminal side of the plasma membrane of brain capillaries in the *in vitro* transport experiment using isolated brain capillaries. Therefore, *in vivo* uptake (or binding) of [^{125}I]E-2078 by the luminal side of brain capillaries was examined using the carotid artery injection technique (12). The *in vivo* extraction of [^{125}I]E-2078 greatly exceeded that of sucrose and showed a significant saturability in the presence of unlabeled peptide (1 mM) in the injectate (table 1). These results suggest that the absorptive-mediated endocytosis could occur at the luminal side of the brain capillaries. Moreover, the transcytosis of proteins through the cerebral endothelium may be *vectorial* (i.e. directed from blood to brain), since the luminal surface but not the abluminal surface exhibits demonstrable endocytotic activity (26,27). Accordingly, the internalization of [^{125}I]E-2078 by isolated brain capillaries might be the result of endocytosis at the luminal surface.

In the development of neuropeptides as neuropharmaceuticals acting on the central nervous system *in vivo*, several factors should be considered in order that systemic administration becomes possible; 1) the stability of the peptide in the systemic circulation, 2) the permeability of the peptide through the blood-brain barrier (BBB), 3) the stability of the peptide in the cytoplasm of endothelial cell and interstitial fluid in the brain. To solve these problems, suitable chemical modifications of the peptide would be the most successful

strategy (4). In this point of view, a novel dynorphin analogue, E-2078, is a peptide that was satisfactorily developed to meet the above factors.

In conclusion, the present study demonstrates that a novel dynorphin analogue, E-2078, is transported by the absorptive-mediated endocytosis system through the BBB without significant metabolism by the brain capillaries. There is a possibility of the permeation of E-2078 through the choroid plexus into cerebrospinal fluid. However, the rapid distribution of circulating substances into brain interstitial space depends on the transport properties of the substance at the BBB, because the surface area of the BBB is much (5,000-fold) greater than that of the blood-cerebrospinal fluid barrier (28). Therefore, it is likely that the absorptive-mediated endocytosis of the peptide at the BBB plays an important role for the permeation of this analgesic peptide from the systemic circulation.

Acknowledgements The authors greatly appreciate Dr. William M. Pardridge for his valuable discussions. The authors thank Mr. Kiminori Okumura for his excellent technical assistance, Drs. Yasuo Miyake and Teruaki Yuzuriha, Research & Development Division, Eisai Co., Ltd. for kindly supplying us with unlabeled and [^{125}I]E-2078 and Mrs. Katsumoto Ume and Saburo Okabe, the Meat Inspection Center of Kanazawa City, for graciously providing us with fresh bovine brains.

REFERENCES

1. A.C. Cuello: Central Distribution of opioid peptides. *Br. Med. Bull.* **39**: 11-16, 1983.
2. S.F. Atwen and M.J. Kuhar,: Distribution and physiological significance of opioid receptors in the brain. *Br. Med. Bull.* **39**: 47-52, 1983.
3. R.A. Houghten, R.W. Swann, and C.H. Li: β-Endorphin: Stability, clearance behavior, and entry into the central nervous system after intravenous injection of the tritiated peptide in rats and rabbits. *Proc. Natl. Acad. Sci. USA* **77**: 4588-4591, 1980.
4. W.M. Pardridge and L.J. Mietus: Enkephalin and blood-brain barrier: Studies of binding and degradation in isolated brain microvessels. *Endocrinology* **109**: 1138-1143, 1981.
5. A. Goldstein, S. Tachibara, L.I. Lowney, M. Hunkapiller, and L. Hood: Dynorphin-(1-13), an extraordinary potent opioid peptide. *Proc. Natl. Acad. Sci. USA* **76**: 6666-6670, 1979.
6. E.A. Barnard and C.D. Mason: Molecular properties of opioid receptors. *Br. Med. Bull.* **39**: 37-45, 1983.
7. T. Nakazawa, M. Mihara, M. Ikeda, T. Kaneko, K. Yamatsu, Y. Arakawa, and S. Tachibana: A novel analogue (E-2078) of dynorphin (2): Analgesia, tolerance and physical dependence. *Int. Narcotic. Res. Conf.* 110, 1987.
8. S. Tachibana, H. Yoshino, T. Arakawa, S. Araki, T. Kaneko, and K. Yamatsu: A novel analogue (E-2078) of dynorphin (1): Design and structure-activity relationship. *Int. Narcotic. Res. Conf.* 60, 1987.
9. K.R. Duffy and W.M. Pardridge: Blood-brain barrier transcytosis of insulin in developing rabbits. *Brain Res.* **420**: 32-38, 1987.

10. J.B. Fishman, J.B. Rubin, J.V. Handrahan, J.R. Connor, and R.E. Fine: Receptor-mediated transcytosis of transferrin across the blood-brain barrier. *J. Neurosci. Res.* **18**: 299-304, 1987.

11. A.K. Kumagai, J.B. Eisenberg, and W.M. Pardridge: Absorptive-mediated endocytosis of cationized albumin and a β-endorphin-cationized albumin chimeric peptide by isolated brain capillaries. *J. Biol. Chem.* **262**: 15214-15219, 1987.

12. W.A. Banks, A.J. Kastin, A.J. Fishman, D.H. Coy, and S.L. Strauss: Carrier-mediated transport of enkephalins and N-tyr-MIF-1 across blood-brain barrier. *Am. J. Physiol.* **251**: E477-E482, 1986.

13. W.H. Oldendorf: Measurement of brain uptake of radiolabeled substances using a tritiated water internal standard. *Brain Res.* **24**: 372-376, 1970.

14. W.M. Pardridge, J. Eisenberg, and T. Yamada: Rapid sequestration and degradation of somatostatin analogues by isolated brain microvessels. *J. Neurochem.* **44**: 1178-1184, 1985.

15. O.H. Lowry, N.J. Rosebrough, A.L. Farr, and R.J. Radall: Protein measurement with the folin phenol reagent. *J. Biol. Chem.* **193**: 265-275, 1951.

16. T.B. Choi and W.M. Pardridge: Phenylalanine transport at the human blood-brain barrier. *J. Biol. Chem.* **261**: 6536-6541, 1986.

17. H.J.L. Frank, W.M. Pardridge, W.L. Morris, R.G. Rosenfeld, and T.B. Choi: Binding and internalization of insulin and insulin-like growth factors by isolated brain microvessels. *Diabetes* **35**: 654-661, 1986.

18. W.M. Pardridge, J. Eisenberg, and J. Yang: Human blood-brain barrier insulin receptor. *J. Neurochem.* **44**: 1771-1778, 1985.

19. W.M. Pardridge: Carrier-mediated transport of thyroid hormones through the rat blood-brain barrier: primary role of albumin-bound hormone. *Endocrinology* **105**: 605-612, 1979.

20. H.S. Wiley and D.D. Cunninghum: The endocytotic rate constant. *J. Biol. Chem.* **257**: 4222-4229, 1982.

21. W.P. Knutson, G.V. Ronnett, and M.D. Lane: Rapid, reversible internalization of cell surface insulin receptors. *J. Biol. Chem.* **258**: 12139-12142, 1983.

22. A.W. Vorbrodt, A.S. Lossinsky, D.H. Dobrogowska, and H.M. Wisniewski: Distribution of anionic sites and glycoconjugates on the endothelial surfaces of the developing blood-brain barrier. *Dev. Brain Res.* **29**: 69-79, 1986.

23. K.R. Duffy, W.M. Pardridge, and R.G. Rosenfeld: Human blood-brain barrier insulin-like growth factor receptor. *Metabolism* **37**: 136-142, 1988.

24. W.M. Pardridge, J. Eisenberg, and J. Yang: Human blood-brain barrier transferrin receptor. *Metabolism* **36**: 892-895, 1987.

25. R.S. Bar, A. DeRose, A. Sandra, M.L. Peacock, and W.G. Owen: Insulin binding to microvascular endothelium: a kinetic and morphometric analysis. *Am. J. Physiol.* **244**: E447-E452, 1983.

26. R.D. Broadwell, B.J. Balin, M. Salcman, and R.S. Kaplan: Brain-blood barrier? Yes and no. *Proc. Natl. Acad. Sci. USA* **80**: 7352-7356, 1983.

27. R.D. Broadwell, B.J. Balin, and M. Salcman: Transcytotic pathway for blood-borne protein through the blood-brain barrier. *Proc. Natl. Acad. Sci. USA* **85**: 632-636, 1988.

28. W.M. Pardridge, H.J.L Frank, E.M. Conford, L.D. Braun, P.D. Crane, and W.H. Oldendorf: Neuropeptides and the blood-brain barrier.

In Neurosecretion and Brain Peptides, ed by J. B. Martin, S. Reichlin, K. L. Bick, pp. 321-328, Raven Press, New York, 1981.

TABLE 1.

Effects of unlabeled E-2078 and L-tyrosine on in vivo brain uptake of [^{125}I]E-2078 in rats[a]

Inhibitor	[^{125}I]E-2078 uptake / [^{3}H]sucrose uptake
	%
None (control)	368 ± 55
Unlabeled E-2078 (1 mM)	185 ± 16**
L-Tyrosine (5 mM)	315 ± 19

[a] Determined by the carotid artery injection technique (Oldendorf, 1970). The values are the means ± S.E. of five experiments.

** Significantly different from control at $p < 0.01$ by Student's t-test.

FIGURE LEGENDS

Fig. 1. *HPLC chromatograms of [^{125}I]E-2078 after incubation with isolated bovine brain capillaries.*

[^{125}I]E-2078 was incubated with bovine brain capillaries for 30 min at 37°C. The supernatant of the incubation mixture was applied into the reversed-phase HPLC column (μ-Bondapak C_{18}). The solvents used were mixtures of water and acetonitrile containing 0.065% TFA. The loaded samples were eluted with a linear gradient of acetonitrile from 20 to 35% within 15 min, followed by a linear gradient of acetonitrile from 35 to 60% within next 5 min. The solvent flow rate was 1.5 ml/min. The radioactivity in each eluent (1 ml) was counted. A HPLC chromatogram of a standard sample of [^{125}I]E-2078 is illustrated in inset.

Fig. 2. *Effect of acid wash period on the acid resistant binding of [^{125}I]E-2078 to isolated bovine brain capillaries.*

[^{125}I]E-2078 (0.4 μM) was incubated with brain capillaries at 37°C for 30 min in the incubation buffer (141 mM NaCl, 4 mM KCl, 2.8 mM $CaCl_2$, 1 mM $MgSO_4$, 10 mM HEPES, 10mM D-glucose, 0.1% bovine serum albumin, pH 7.4). The incubation mixture was centrifuged at 10,000 x g for 45 sec, the resultant pellet was resuspended and incubated with 400 μl of ice cold acetate-barbital buffer (pH 3.0) for designated time intervals (1, 3, 6, 10 min), and the suspension was centrifuged at 10,000 x g for 45 sec. The pellet was dissolved in 500 μl of 1 N NaOH at 60°C for 10 min and the radioactivity was counted. The percentage of acid resistant binding to the total binding was plotted against the acid wash period. Each point represents the mean ± S.E. of three experiments.

Fig. 3. *Time courses of the total and acid resistant bindings of [^{125}I]E-2078 to isolated bovine brain capillaries.*

After incubation of [^{125}I]E-2078 with brain capillaries at 37°C for 30 min, the incubation mixture was centrifuged at 10,000 x g for 45 sec and the supernatant was counted. The pellet was resuspended and incubated with 400 μl of ice cold acetate-barbital buffer (pH 3.0) for 6 min, and the suspension was centrifuged at 10,000 x g for 45 sec. The pellet was dissolved by 500 μl of 1 N NaOH at 60°C for 10 min and centrifuged at 10,000 x g for 45 sec. The acid soluble radioactivity in the supernatant and the acid resistant radioactivity in the pellet were counted. The total (o) and acid resistant (●) bindings were expressed as the cell-to-medium concentration (cell/medium) ratios by calculation using eqs. 1 and 2 in the text, respectively. Each point represents the mean ± S.E. of three experiments.

Fig. 4. *Effect of temperature on the acid resistant binding of [^{125}I]E-2078 to isolated bovine brain capillaries.*

After incubation of [^{125}I]E-2078 with brain capillaries at 37°C (o) or 4°C (●) for 30 min, the acid resistant binding was determined (as cell/medium ratio) as described in the legend to figure 3. Each point represents the mean ± S.E. of five experiments.

Fig. 5. *The effect of increasing osmolarity of the incubation buffer on the internalization of [^{125}I]E-2078 (0.4 μM) by normal and collapsed brain capillaries.*

Brain capillaries were preincubated for 5 min at 37°C in the

incubation buffer with (1,400 mOsm; ●) or without (300 mOsm; O) 1 M sucrose. The acid resistant binding was measured (as cell/medium ratio) as described in the legend to figure 3. Each point represents the mean ± S.E. of three experiments.

Fig. 6. *Effect of phenylarsine oxide preloading on the internalization of [^{125}I]E-2078 by isolated bovine brain capillaries.*

Bovine brain capillaries were preincubated for 20 min at 37°C in the incubation buffer with (●) or without (O) 10 μM phenylarsine oxide. The acid resistant binding was determined (as cell/medium ratio) as described in the legend to figure 3. Each point represents the mean ± S.E. of three experiments.

Fig. 7. *Concentration dependence of the surface binding of [^{125}I]E-2078 to isolated bovine brain capillaries.*

[^{125}I]E-2078 (0.4 μM) and various concentrations of unlabeled E-2078 were incubated with brain capillaries (approximately 3 mg/ml) at 37°C for 30 min in the incubation buffer. The acid soluble binding (as cell/medium ratios) were determined as described in "Materials and Methods. The inset presents the Scatchard plot of the saturable surface binding of [^{125}I]E-2078, where saturable surface binding was obtained from the surface binding minus non-saturable surface binding which was determined in the presence of 10 mM unlabeled E-2078. Each point represents the mean ± S.E. of five experiments.

Fig. 8. *Effects of several inhibitors on the total and acid resistant bindings of [^{125}I]E-2078 to isolated bovine brain capillaries.*

Brain capillaries were preincubated for 5 min at 37°C with either 10 μM of insulin, 10 μM of holotransferrin, 1 mM of dynorphin(1-8), 1 mM of β-neoendorphin, 10 μM of naloxone, 300 μM of polylysine, 300 μM of protamine or 300 μM of polyglutamate. Subsequently, the total (left panel) and acid resistant (right panel) bindings (as percent of control) were determined as described in the legend to figure 3. Each point represents the mean ± S.E. of five experiments.

Fig. 1

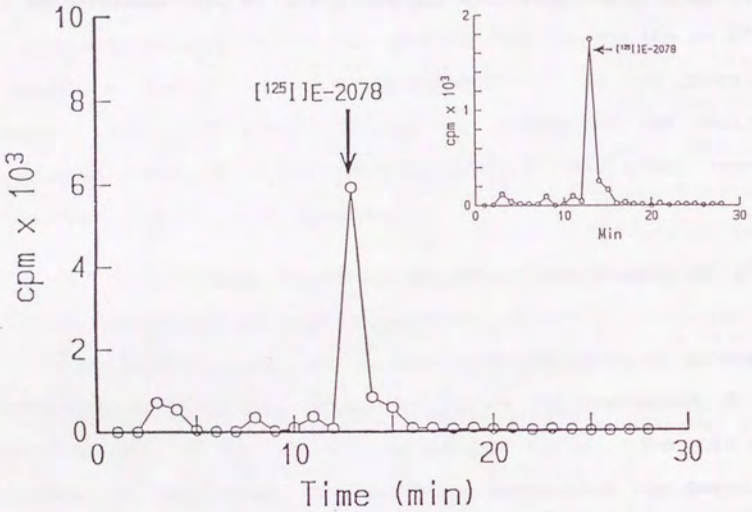
[125]I-2078
cpm x 10^3
Time (min)
0
2
4
6
8
10
0
10
20
30
cpm x 10^3
Min

Fig. 2

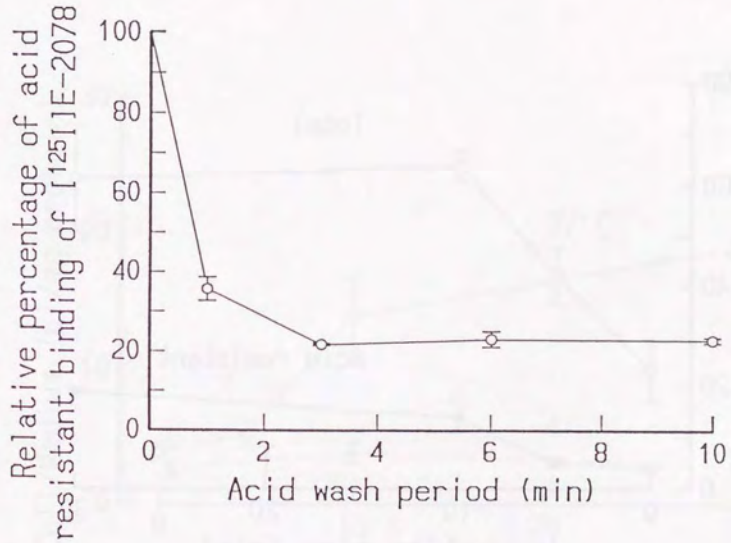
Relative percentage of acid resistant binding of [125]I-2078
Acid wash period (min)
0
20
40
60
80
100
0
2
4
6
8
10

Fig. 3

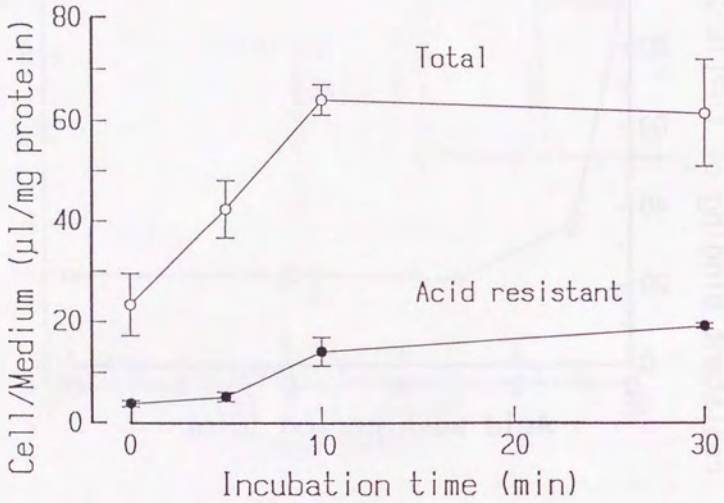
Cell/Medium (µl/mg protein)
80
60
40
20
0
Total
Acid resistant
0
10
20
30
Incubation time (min)

Fig. 4

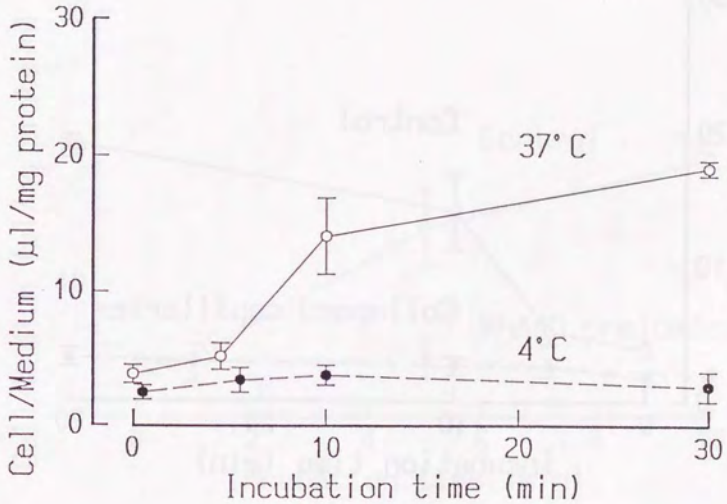
Cell/Medium (µl/mg protein)
30
20
10
0
37°C
4°C
0
10
20
30
Incubation time (min)

Fig. 5

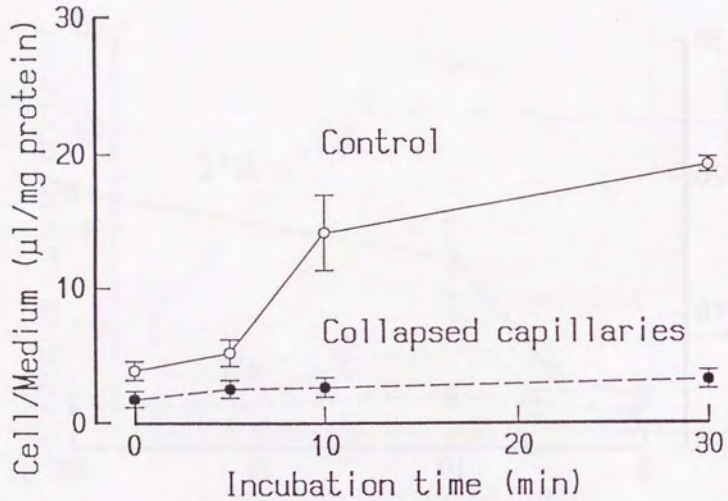
Cell/Medium (µl/mg protein)
30
20
10
0
Control
Collapsed capillaries
0
10
20
30
Incubation time (min)

Fig. 6

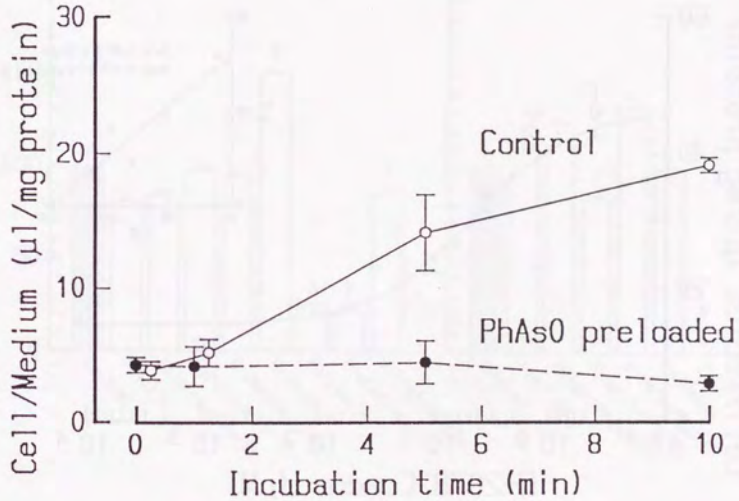
Cell/Medium (µl/mg protein)
30
20
10
0
Control
PhAsO preloaded
0
2
4
6
8
10
Incubation time (min)

Fig. 7

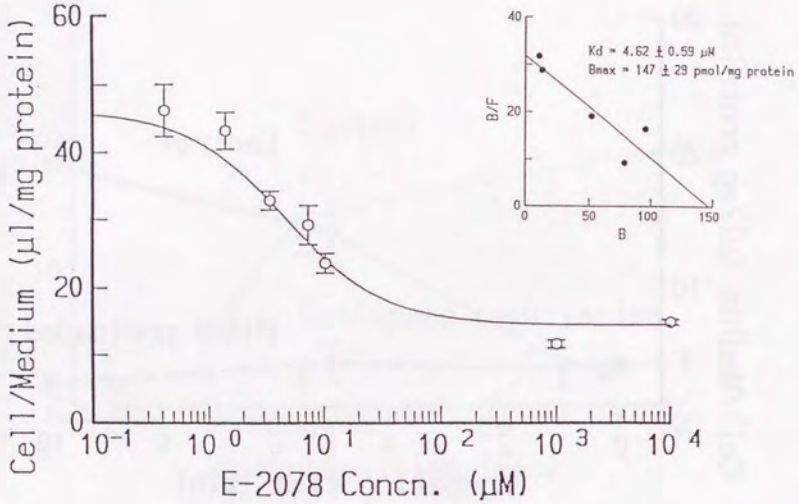
Cell/Medium (µl/mg protein)
60
40
20
0
10⁻¹
10 0
10 1
10 2
10 3
10 4
E-2078 Concn. (µM)
Kd = 4.62 ± 0.59 µM
Bmax = 147 ± 29 pmol/mg protein
B/F
40
20
0
0
50
100
150
B

Fig. 8

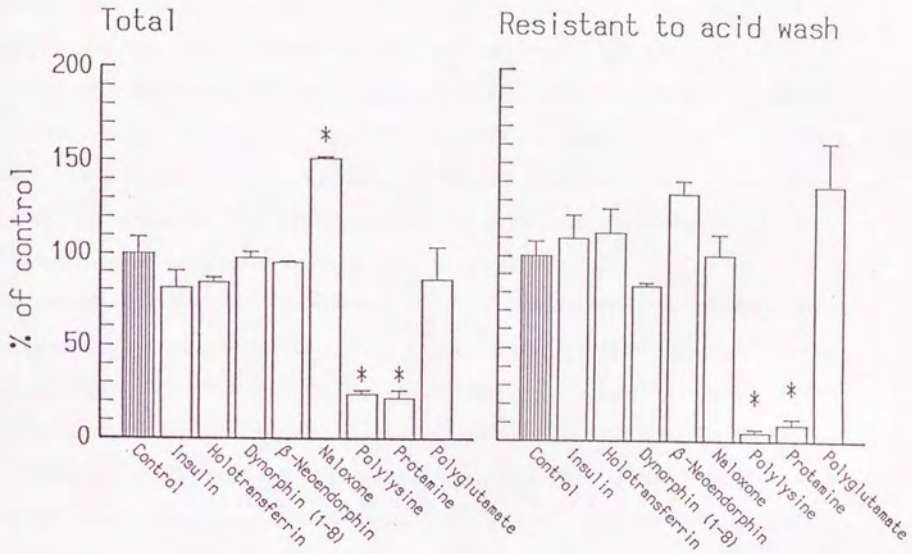
Total
Resistant to acid wash
% of control
200
150
100
50
0
Control
Insulin
Holotransferrin
Dynorphin (1-8)
β-Neoendorphin
Naloxone
Polylysine
Protamine
Polyglutamate

PART VI

AN APPLICATION OF HIGH-PERFORMANCE LIQUID CHROMATOGRAPHY IN DISPOSITION STUDY OF A_{14}-^{125}I-INSULIN IN MICE

SUMMARY

In order to describe quantitatively the *in vivo* distribution and elimination of insulin, HPLC separation was applied to the pharmacokinetic study of human insulin ^{125}I-labeled at tyrosine-A_{14} (A_{14}-^{125}I-insulin) as a tracer. Intact A_{14}-^{125}I-insulin was determined by HPLC and TCA-precipitation in plasma and various tissues after its intravenous bolus injection into mice. TCA-precipitation consistently overestimated the intactness of A_{14}-^{125}I-insulin compared with HPLC, possibly due to the presence of both a TCA-precipitable, intermediate degradation product of labeled insulin found in HPLC elution profiles and reported high-molecular-weight forms of labeled insulin in plasma. Thus, TCA-precipitation gave a considerably lower total plasma clearance (CL_{tot}) value than HPLC.

The half-life of A_{14}-^{125}I-insulin was prolonged by a simultaneous injection of unlabeled insulin (8 U/kg), and labeled insulin behaved similarly with ^{14}C-inulin (an extracellular fluid marker). The concentration-time profiles of HPLC-separated labeled insulin in plasma were analyzed by a noncompartmental moment method, and it was found that both plasma clearance (CL_{tot}) and steady-state apparent distribution volume (Vd_{ss}) of A_{14}-^{125}I-insulin were considerably decreased by unlabeled insulin coadministration. Especially, Vd_{ss} of labeled insulin decreased by 79% to be similar to that of inulin (181 ml/kg), suggesting that the nonspecific binding of labeled insulin to tissues was so small that Vd_{ss} of labeled insulin reduced to the extracellular fluid volume (approximately 20% of the body weight) when its receptor binding was blocked effectively by unlabeled insulin. This observation, together with 63% reduction of CL_{tot} by unlabeled insulin coadministration, demonstrates that saturable, receptor-

mediated processes of distribution and elimination are essentially involved in the pharmacokinetics of HPLC-separated A_{14}-^{125}I-insulin.

INTRODUCTION

Recently, high-performance liquid chromatography (HPLC) has been successfully employed not only to purify authentic insulin (1) and monoiodinated insulin isomers (2,3) but also to separate the degradation products of labeled insulin generated by isolated hepatocytes (4,5) or proteases (5,6). Previous *in vitro* studies (4-9) have indicated that TCA-precipitable, insulin-sized intermediate products of insulin appear to derive from cell-associated processes. After degradation by human fibroblast, separation of insulin-sized products of insulin could be readily accomplished by HPLC, but not by other methods (9). In contrast, a great number of *in vivo* kinetic studies of insulin have been performed almost exclusively by the use of radioimmunoassay (RIA), gel filtration and TCA-precipitation, but have not been evaluated quantitatively by HPLC analysis.

In the field of pharmacokinetics, there is now a growing body of evidence demonstrating the important roles of receptor binding in distribution and elimination of peptide hormones (10-12) including insulin (13-15), due to hormone-receptor binding and subsequent cellular events (receptor-mediated internalization and degradation) which have been studied extensively using isolated cells (16,17). With regard to the receptor binding activity of radiolabeled insulin, it has been reported that HPLC-purified A_{14}-monoiodoinsulin is indistinguishable from native insulin (18), and that B-chain-labeled insulins show higher affinity than A_{14}-monoiodoinsulin in adipocytes possibly due to the alterations in either receptor binding and cooperative interactions, because tyrosines of the B-chain are believed to be close or within the binding site (19). However, most previous studies on the fate of labeled insulin have been performed

using heterogenously labeled insulins, except for the study by Philippe *et al.* (14), who used tritiated insulin assayed by gel chromatography, and a recent study by Cockram *et al.* (20) who utilized A_{14}- and B_1-labeled insulin tracers to investigate the mechanisms of intracellular processing of insulin *in vivo* by the use of TCA-precipitation and immunoprecipitation, although they did not measure directly the intracellular degradation products of insulin.

In the present study, therefore, we quantitatively compared the intactness of A_{14}-^{125}I-insulin between the HPLC-separation and TCA-precipitation methods, and examined the concentration profiles of HPLC-separated A_{14}-^{125}I-insulin in plasma and in various tissues after its intravenous injection in mice.

MATERIALS AND METHODS

Reagents. Human insulin ^{125}I-labeled at tyrosine-A_{14} (A_{14}-^{125}I-insulin), with a specific activity of 2,000 Ci/mmol, and ^{14}C-inulin carboxylic acid with a specific activity of 2-10 mCi/mmol were purchased from the Radiochemical Center (Amersham, Arlington Heights, Illinois). Crystalline porcine insulin and bovine serum albumin (BSA, Fraction V) were obtained from Sigma Chemical Co. (St. Louis, Missouri), and trichloroacetic acid (TCA) and trifluoroacetic acid (TFA) from Wako Pure Chemical Industries, Ltd. (Osaka, Japan). All other reagents were commercially available and of analytical grade. The monoiodinated insulin was dissolved in phosphate buffered saline (PBS) containing 0.1% BSA (designated as PBS solution) and stored at -20°C until study. The purity of the labeled insulin was at least 95% pure as assayed by a high-performance liquid chromatography (HPLC).

Insulin Administration and Sampling. Adult male ddY mice (Sankyo Laboratory Co., Ltd., Toyama, Japan) weighing 30-38 g were used throughout the experiments without fasting. Under light anesthesia with ether, the mice were kept in the spine position on a fixed board and the body temperature was maintained at 37°C by heating lamps. The jugular vein was cannulated with polyethylene tubing (SP-10; o.d. 0.61 mm, i.d. 0.28 mm; Natsume Seisakusho, Co., Tokyo, Japan) for administration of labeled insulin, and a loose ligature (surgical string) was placed around the carotid artery for blood sampling. After recovery from anesthesia, 6.5 μCi/kg of A_{14}-^{125}I-insulin (without and with 8 U/kg of unlabeled porcine insulin) plus saline up to 50 μl was rapidly injected through the jugular vein using a microsyringe attached to the cannula. When unlabeled insulin was coadministered, glucose was infused constantly at a rate of 24

mg/min/kg to maintain euglycemia. At designated times after intravenous injection of labeled (and unlabeled) insulin, the carotid artery was gently pulled upward using the string and dissected for collection of blood into heparinized tubes, from which plasma was separated by centrifugation. The liver, kidney, lung, spleen and gut (first third of the small intestine) were quickly excised, rinsed with ice-cold saline, and blotted dry. Each tissue was precisely weighed and quickly added to 1 ml of ice-cold 1 M acetic acid solution containing 6 M urea (designated as AcOH solution). After total ^{125}I-radioactivity was counted in a γ-counter (ARC-605; Aloka Co., Tokyo, Japan), each tissue was homogenized in a motor-driven Potter homogenizer at 4°C. The tissue homogenates were then centrifuged at 12,000 rpm for 20 min in a microcentrifuge (RL-500SP; Tomy Seiko Co., Ltd., Tokyo, Japan) at 4°C and the supernatants (designated as tissue samples) were transferred to separate tubes. The radioactivity recovered in the supernatant was more than 80% of the total radioactivity. A_{14}-^{125}I-Insulin in plasma and tissue samples was assayed by TCA-precipitation method or HPLC method as described later. Plasma glucose concentrations were measured by a glucose peroxidase method (21) using a commercial kit (Glucose B-Test, Wako Pure Chemical Industries, Ltd.). Plasma insulin concentrations were determined by RIA using a commercial kit (IRI Eiken; Eiken Chemical Co., Ltd., Tokyo, Japan).

In order to compare the pharmacokinetic behaviors between insulin and inulin (an extracellular fluid marker), ^{14}C-inulin (30 µCi/kg), of which molecular weight (5,200 dalton) is close to that of insulin, was intravenously injected through the cannulated jugular vein, and blood

was sampled at designated times, as performed previously in rats (22) and rabbits (23). The obtained plasma samples were oxidized with a sample oxidizer (ASC-113; Aloka Co.) to $^{14}CO_2$, and the radioactivity was determined by a liquid scintillation counter (LSC-700; Aloka Co.).

Analytical Procedures. Intactness of A_{14}-^{125}I-insulin in plasma and various tissues were determined by trichloroacetic acid (TCA)-precipitation and HPLC as follows. For TCA-precipitation, plasma samples (100 µl) were mixed well with 1 ml of 5% (w/v) TCA solution. Similarly, tissue samples (1 ml) were mixed well with an equal volume of 10% (v/v) TCA solution. These mixtures were kept standing at 4°C for 30 min, centrifuged at 1,500 x g for 15 min, and the supernatant was transferred to a separate tube by aspiration. The percentage of radioactivity in precipitate (designated as TCA-precipitable percent) was calculated as (cpm in precipitate)/[(cpm in precipitate)+(cpm in supernatant)] x 100.

For HPLC, plasma samples (100 µl) were mixed vigorously with an equal volume of ethanol, centrifuged at 10,000 x g for 20 min in a microcentrifuge (RL-500SP), and the supernatant was filtered through a Millipore filter (0.45 µm; Nihon Millipore Kogyo, Yonezawa, Japan). The percent of the radioactivity extracted from the samples by ethanol was approximately 90%. Fifty µl of the resultant supernatant was loaded onto a reversed-phased HPLC column, µ-Bondapak C_{18} (30 cm x 3.9 mm i.d.; Waters Associates, Inc., Milford, Massachusetts). The constant-flow solvent delivery system, LC-6A (Shimadzu Corp., Kyoto, Japan) was equipped with an ultraviolet detector, SPO-6A (Shimadzu Corp.) and a gradient programmer, SCL-6A (Shimadzu Corp.). A guard column, C_{18} CORASIL (Waters Associates, Inc.) was placed between the injector and the analytical column. The mobile phase consisted of two

solvents. Solvent A was a mixture of water and TFA 0.1% (v/v) and solvent B a mixture of acetonitrile and TFA 0.1% (v/v). After an isocratic run at 25% solvent B for 5 min, a linear gradient was run from 25% to 40% solvent B for 10 min, and 40% solvent B was hold for 15 min. The solvent flow rate was 1.0 ml/min. The column and solvents were kept at room temperature. The radioactivity in each sample (1 ml) was counted in a γ-counter.

Tissue samples (homogenate supernatants) were lyophilized and reconstituted in approximately 200 µl of a mixture of acetonitrile and water (25:75, v/v). Subsequent procedure was the same as that described above for plasma samples.

The percentage of the radioactivity associated with intact A_{14}-^{125}I-insulin in plasma and tissue samples was calculated by measuring the peak areas eluted from the column. The total radioactivity eluted from the column was more than 90% of the radioactivity loaded onto the column.

Data Analysis. Intact percent of A_{14}-^{125}I-insulin in plasma and tissue samples was expressed in terms of HPLC by using the relationship between the TCA-precipitation and HPLC methods. Plasma concentrations (Cp) of A_{14}-^{125}I-insulin and ^{14}C-inulin were expressed as percent of dose per ml plasma. Especially, Cp of labeled insulin was calculated by the following equation:

$$Cp = (\text{total cpm/ml plasma}) \times (\text{intact percent in plasma})/\text{Dose}/100 \quad (1)$$

where Dose represents (intact cpm administered)/(kg body weight).

Plasma concentration *versus* time curves of A_{14}-^{125}I-insulin and ^{14}C-inulin were analyzed by a non-compartmental moment method (24). Total plasma clearance (CL_{tot}) and the steady-state apparent volume of

distribution (Vd_{ss}) were calculated by the following equations, respectively:

$$CL_{tot} = \text{Dose}/AUC \quad (2)$$

$$Vd_{ss} = \text{Dose} \cdot AUMC/AUC^2 \quad (3)$$

where AUC and AUMC are the area under the plasma concentration *versus* time curve and the area under the product of time (t) and the plasma concentration *versus* time curve, respectively. AUC and AUMC were calculated by the trapezoidal rule with extrapolation to infinite time (24). CL_{tot} and Vd_{ss} of A_{14}-^{125}I-insulin and ^{14}C-inulin were compared by means of the one-way analysis of variance (ANOVA), followed by the Student's *t*-test, among the three groups of mice injected with; 1) a tracer dose of A_{14}-^{125}I-insulin; 2) a tracer dose of A_{14}-^{125}I-insulin with unlabeled insulin (8 U/kg); and 3) a tracer dose of ^{14}C-inulin.

RESULTS

Figure 1A shows a representative HPLC elution profile of standard A_{14}-^{125}I-insulin and indicates that the monoiodinated insulin used was a highly purified preparation. Figures 1B-1D show representative HPLC elution profiles of A_{14}-^{125}I-insulin and its degradation products from plasma, kidney and liver 15 min after intravenous bolus injection into mice. Among the major three peaks of radioactivity observed, the first peak probably corresponds for the most part to $^{125}I^-$ and in part to ^{125}I-tyrosine, in view of the findings of Sodoyez *et al.* (25) whose studies demonstrated a very rapid dehalogenation of ^{125}I-tyrosine *in vivo*. The second peak corresponds to an intermediate degradation product of labeled insulin, and the third to intact A_{14}-^{125}I-insulin.

Figure 2 illustrates a curvilinear relationship of intact percent of labeled insulin between the TCA-precipitation and HPLC-separation methods, indicating that TCA-precipitation consistently overestimates the intactness of A_{14}-^{125}I-insulin in plasma and tissues, possibly due to the nonspecific adsorption of TCA-soluble fragments including ^{125}I-iodide to the pellet and to the presence of an intermediate degradation product (Figs. 1B-1D) which was approximately 80% precipitable by 5% TCA. There was a decrease with time in the peak area associated with A_{14}-^{125}I-insulin and a corresponding increase in the area of the first peak, and therefore, the intactness of A_{14}-^{125}I-insulin decreased with time in plasma and tissues after its intravenous injection, as inspected from Figure 2. By utilizing this correlation between the two methods, it was clearly shown that the plasma concentrations *versus* time curves of HPLC-separated A_{14}-^{125}I-insulin after its iv injection (Fig. 3B) differed distinctly from those of TCA-precipitable A_{14}-^{125}I-insulin (Fig. 3A). Using a

noncompartmental moment analysis (24), CL_{tot} and Vd_{ss} of TCA-precipitable A_{14}-^{125}I-insulin were determined to be 3.06 ml/min/kg and 1332 ml/kg, respectively. On the other hand, CL_{tot} and Vd_{ss} of HPLC-separated A_{14}-^{125}I-insulin were determined to be 45.1 ml/min/kg and 1204 ml/kg, respectively, as listed in Table 1. Thus, the TCA-precipitation method gave a considerably lower CL_{tot} and a slightly higher Vd_{ss} than the HPLC method.

Basal glucose and insulin concentrations in plasma were 2.59 $\pm$ 0.14 mg/ml (mean $\pm$ SEM, n=11) and 1.96 $\pm$ 0.25 ng/ml (mean $\pm$ SEM, n=11), respectively. With glucose infusion, plasma glucose levels after 30 min in mice injected with unlabeled insulin (8 U/kg) were not significantly different from those in mice injected with tracer insulin injection, although it was not confirmed whether this euglycemic condition continuously maintained throughout the experiment. However, from the observation that highly dosed insulin behaved similarly with inulin (Figs. 3B and 3B), which was an extracellular marker as verified previously in rats (22) and rabbits (23), it is likely that the *in vivo* receptor binding of A_{14}-^{125}I-insulin was almost completely displaced by a high dose of unlabeled insulin. Therefore, possible alterations in endogenous insulin secretion, caused by either hyperglycemia or hypoglycemia during intravenous glucose infusion after unlabeled insulin injection, will not affect the pharmacokinetics of A_{14}-^{125}I-insulin in this condition.

The plasma concentrations of HPLC-separated A_{14}-^{125}I-insulin and ^{14}C-inulin were analyzed by a noncompartmental moment method (24), and the obtained pharmacokinetic parameters (CL_{tot} and Vd_{ss}) and their standard deviations are listed in Table 1. Here, the extrapolation of

observed data to infinite time was performed to evaluate the terminal slope by using a least-squares regression line generated from the data points over 10-30 min. ANOVA indicated that the differences in CL_{tot} and Vd_{ss} among the three plasma concentration vs. time curves in mice were significant at 1% level. As presented in Table 1, CL_{tot} (16.5 ml/min/kg) and Vd_{ss} (251 ml/kg) of labeled insulin at the high dose were considerably lower than those of tracer insulin, but similar to those of ^{14}C-inulin, 11.3 ml/min/kg and 181 ml/kg, respectively. The Student's *t*-test at the 1% significant level revealed that CL_{tot} and Vd_{ss} values are significantly different between any combinations of the three groups, except that Vd_{ss} values are not significantly different between the mice injected with A_{14}-^{125}I-insulin at a high dose of unlabeled insulin and ^{14}C-inulin.

DISCUSSION

The close correlation between the receptor binding activity and the extent of elimination and tissue distribution after intravenous administration has been demonstrated for some peptide hormones (10-15) including insulin. This correlation should be considered in pharmacokinetic studies of endogenous peptides and proteins, because of the following possible consequences: 1) a tracer with decreased affinity shows decreased distribution volumes and plasma clearances, and 2) a tracer with high affinity shows dose-dependent, nonlinear pharmacokinetics at such doses that saturate its receptors, while a tracer with low affinity shows dose-independent, linear pharmacokinetics. Unfortunately, differences in the affinity of tracers and in the doses of insulin (or the plasma insulin levels), together with differences in assay methods employed, have made it difficult to comprehensively integrate a great number of pharmacokinetic information on the distribution volume and clearance values of insulin reported previously from different laboratories.

In the present study, a rapid HPLC method was applied to the study of *in vivo* distribution and elimination of A_{14}-^{125}I-insulin in mice. The use of tracer with a high specific activity enabled us to examine the disposition of exogenously administered insulin with no interference with endogenous insulin in plasma and tissues. Moreover, A_{14}-monoiodinated insulin used was reported to show equipotency with native insulin in isolated adipocytes (18). Thus, the distribution and elimination of A_{14}-^{125}I-insulin (without unlabeled insulin injection) could be the consequence of physiological interactions of labeled insulin with its receptors and degradation enzymes in target tissues such as liver, muscle and adipose.

Previous *in vitro* studies (4-9) found that TCA-precipitable, insulin-sized intermediate products of insulin were generated by the interaction of insulin with degrading proteases in cytosol (5,6) and on the external surface of the cell membrane (7-9). Among the assay methods of endogenous and exogenous insulins, RIA recognizes a certain immunoreactive portion of the insulin molecule so that it cannot distinguish between intact insulin and intermediate products of insulin. Similarly, TCA-precipitation method, although very rapid and easy to carry out, recognizes various-sized fragments of peptides that can be precipitable in TCA solution, so that it cannot separate high-molecular-weight (HMW) forms and intermediate products of insulin from intact insulin. Since HMW radioactive insulin exhibited a prolonged half life compared with monocomponent insulin (26), it follows that TCA-precipitation inevitably gives small values of CL_{tot} and Vd_{ss} of A_{14}-^{125}I-insulin comparable to that of ^{14}C-inulin (Fig. 3), in spite of the fact that insulin is eliminated from plasma not only by renal glomerular filtration but also by metabolism by liver and muscle under physiological conditions (27). Moreover, TCA-precipitation gave the CL_{tot} values of A_{14}- and B_1-labeled insulin tracers approximately one-half of those obtained by immunoprecipitation in dogs (20), suggesting the presence of insulin molecular fragments that retain little immunoreactivity but high TCA-precipitability because of sufficient molecular size. These lines of evidence lend proof to the lack of reliability to estimate the CL_{tot} and Vd_{ss} values of labeled insulin by the use of TCA-precipitation method.

In *in vitro* experiments, separation of the various fragments of insulin, particularly that of insulin-sized products, can be readily

accomplished by reversed-phase HPLC (6,9). In the present *in vivo* study, the HPLC elution profiles (Figs. 1B-1D) indicate that there are at least two products of A_{14}-labeled insulin less hydrophobic than intact insulin in plasma and tissues after intravenous injection in mice. The peak eluting near intact insulin presumably represents insulin-sized intermediate products, because it was TCA-precipitable by approximately 80%. From this point of view, HPLC analysis appears to be more reliable than other methods for the measurement of intact A_{14}-^{125}I-insulin in biological samples of *in vivo* studies as well as those of *in vitro* studies. However, since it is too laborious to analyze a number of biological samples by HPLC, we routinely employed the TCA-precipitation method, then the obtained TCA-precipitability was converted into the intact percent of the HPLC method, using the correlation between these two methods (Fig. 2). With this approach, a high TCA-precipitability (e.g., more than 90%) may not cause a significant change in insulin concentrations, while a low TCA-precipitability (e.g., lower than 15%) may cause a wide variation in estimating the HPLC-intactness from the calibration curve presented in Fig. 2. This is why we did not analyze the plasma concentrations of A_{14}-^{125}I-insulin at the times longer than 30 min after iv injection, when TCA-precipitability of ^{125}I-insulin in plasma samples fell close to the unreliable lower extreme of the curve.

Since liver is the major eliminating organ of insulin *in vivo*, the result of HPLC separation of biological samples could be compared with that of Hamel *et al.* (4), who have shown by HPLC that two insulin-sized intermediate products were generated in hepatocytes incubated with A_{14}-^{125}I-insulin at 37°C, whereas a single intermediate product was found in the incubation medium. On the contrary, in the present

study, only one intermediate product of A_{14}-^{125}I-insulin was separated by HPLC from the liver and plasma samples (Fig. 1). This is possibly because the retention time of labeled insulin in this study (23 min) is so short compared with that in the study of Hamel *et al.* (4) (55 min) that our HPLC analysis could not detect the "doublets", a pair of insulin-sized materials, that eluted from their HPLC system in close positions (19- and 23-min) (4). However, considering that some degradation occurs on the membrane (28), we cannot exclude the possibility that one of the above-mentioned doublets is ascribed to extracellular degradation, and the generated intermediate product was washed out from the extracellular space by the rapid blood flow before partitioning into hepatocytes, while even a slow uptake of the product by hepatocytes may proceed in *in vitro* condition where cells are surrounded by the same incubation medium.

The good recovery (more than 80%) of A_{14}-^{125}I-insulin extraction from tissues (in 1 M AcOH and 6 M urea) may well be explained not only by the effects of a low pH and urea in homogenates which effectively dissociate insulin from its receptors (29), but also by the effect of urea to dissociate degraded insulin fragments noncovalently bound to certain tissue components, as previously demonstrated for ^{125}I-nerve growth factor (30). TCA-precipitabilities (%) of labeled insulin in the pellets were almost equal to those in the supernatants after centrifugation of tissue homogenates in AcOH solution, suggesting that at most 20% loss of radioactivity during the extraction from tissue samples was not due to specific binding of labeled insulin to certain cellular components, but due to nonspecific adsorption to the pellets. In this study of rapid HPLC analysis, we preferred a simple method of

extraction of radioactive materials to other procedures that may give consistently higher yields. Moreover, since ethanol does not precipitate free insulin but insulin-receptor complex (31), it could be reasonable that A_{14}-^{125}I-insulin was recovered well, after tissue homogenates were deproteinized with ethanol in the presence of urea at a low pH (in acetic acid). Taken altogether, the good recovery of the labeled insulin in the above pretreatment procedures made it possible to quantitatively evaluate the *in vivo* disposition of insulin by the use of HPLC.

The large Vd_{ss} value (approximately 120% of the body weight) of A_{14}-^{125}I-insulin at a tracer dose suggests that insulin is not only distributed to the extracellular fluid but also reversibly bound to its binding sites (receptors) in target tissues at the physiological concentrations of plasma insulin. In contrast, when a high dose of unlabeled insulin was simultaneously injected, A_{14}-^{125}I-insulin behaved similarly with ^{14}C-inulin (Fig. 3). The pharmacokinetic analysis revealed that Vd_{ss} of labeled insulin decreased significantly by 79% with a simultaneous injection of unlabeled insulin (8 U/kg) to be close to that of inulin (181 ml/min/kg), suggesting that the nonspecific binding of labeled insulin to tissues was so small that Vd_{ss} of labeled insulin reduced to the extracellular fluid volume (approximately 20% of the body weight) when its receptor binding was blocked effectively by unlabeled insulin. Moreover, CL_{tot} of insulin was reduced significantly by 63% with a simultaneous injection of unlabeled insulin, but somewhat higher than that (11.3 ml/min/kg) of ^{14}C-inulin because of the presence of certain nonspecific clearance mechanism(s) other than renal glomerular filtration, which coincides with the presence of non-receptor-mediated clearance found in isolated

rat hepatocytes (17). Very similar result was reported in rats for the initial volume distribution and metabolic clearance of ^{3}H-insulin assayed by gel chromatography (14). From the above findings, it was demonstrated that saturable and receptor-mediated processes of tissue distribution and elimination are involved in the pharmacokinetics of HPLC-separated A_{14}-^{125}I-insulin. The results obtained by HPLC method will be of much importance to relate these *in vivo* pharmacokinetic processes to the physiological and biochemical consequences in a quantitative manner, e.g., transcapillary diffusion, receptor binding, internalization with receptors and intracellular degradation.

In conclusion, HPLC was applied to the pharmacokinetic study of insulin in mice using A_{14}-^{125}I-insulin as a tracer, which retains the same receptor binding activity and biological potency with native insulin. HPLC elution profiles from both plasma and tissues indicated the presence of at least two products of insulin in plasma and tissues more hydrophilic than intact insulin, and the TCA-precipitable material, which eluted close to intact insulin, might be one of the insulin-sized intermediate products reported in previous *in vitro* studies using isolated hepatocytes and adipocytes. Further characterization of the radioactivity associated with each peak would give more information on the mechanisms of intracellular processing of insulin *in vivo*, but is beyond the scope of the present study. Accordingly, the present study must be viewed as a first step of HPLC application to the study of *in vivo* disposition of insulin.

ACKNOWLEDGMENTS This study was supported by a grant-in-aid for Scientific Research from the Ministry of Education, Science and Culture of Japan, Project Research Fund from the Graduate School of Natural Science and Technology, Kanazawa University, and grants from Takeda Science Foundation and Nakatomi Health Science Foundation.

REFERENCES

1. I.S. Johnson: Authenticity and purity of human insulin (recombinant DNA). *Diabetes Care* **5** (Suppl.), 4-12 (1982).

2. F.B. Stenz, R.K. Wright, and A.E. Kitabchi: A rapid means of separating A_{14}-^{125}I-insulin from heterogeneously labeled insulin molecules for biologic studies. *Diabetes* **31**, 1128-1131 (1982).

3. B.H. Frank, D.E. Peavy, C.S. Hooker, and W.C. Duckworth: Receptor bindig properties of monoiodotyrosyl insulin isomers purified by high performance liquid chromatography. *Diabetes* **32**: 705-711, 1983.

4. F.G. Hamel, E.D. Peavy, M.P. Ryan, and W.C. Duckworth: HPLC analysis of insulin degradation products from isolated hepatocytes. *Diabetes* 36, 702-708 (1987).

5. W.C. Duckworth, F.G. Hamel, D.E. Peavy, J.J. Liepnieks, M.P. Ryan, M.A. Hermodson, and B.H. Frank: Degradation products of insulin generated by hepatocytes and by insulin protease. *J. Biol. Chem.* 263, 1826-1833 (1988).

6. F.G. Hamel, D.E. Peavy, M.P. Ryan, and W.C. Duckworth: High performance liquid chromatographic analysis of insulin degradation by rat skeletal muscle insulin protease. *Endocrinology* **118**, 328-333 (1986).

7. W.G. Blackard, C. Ludeman, and J. Stillman: Role of hepatocytes plasma membrane in insulin degradation. *Am. J. Physiol.* **248**, E194-E202 (1985).

8. O. Sonne: Receptor-mediated degradation of insulin in isolated rat adipocytes. Formation of a degradation product slightly smaller than insulin. *Biochim. Biophys. Acta* **927**, 106-111 (1987).

9. F.B. Stenz, H.L. Harris, and A.E. Kitabchi: Early detection of degraded A_{14}-^{125}I-insulin in human fibroblasts by the use of high performance chromatography. *Diabetes* **32**, 474-477 (1983).

10. R.E. Weitzman and D.A. Fisher: Arginine vasopressin metabolism in dogs. I. Evidence for a receptor-mediated machanism. *Am. J. Physiol.* **235**, E591-E597 (1978).

11. H. Sato, Y. Sugiyama, Y. Sawada, T. Iga, and M. Hanano: In vivo evidence for the specific binding of human β-endorphin to the lung and liver of the rat. *Biochem. Pharmacol.* **37**, 2273-2278 (1988).

12. D.C. Kim,, Y. Sugiyama, H. Satoh, T. Fuwa, T. Iga, and M. Hanano: Kinetic analysis of in vivo receptor-dependent binding of human epidermal growth factor by rat tissues. *J. Pharm. Sci.* **77**, 200-207, 1988

13. M. Berman, E.A. McGuire, J. Roth, and A.J. Zeleznik: Kinetic modeling of insulin binding to receptors and degradation in vivo in the rabbit. *Diabetes* **29**, 50-59 (1980).

14. J. Philippe, P.A. Halban, A. Gjinovci, W.C. Duckworth, J. Estreicher, and A.E. Renold: Increased clearance and degradation of [^{3}H]insulin in streptozotocin diabetic rats: Role of the insulin-receptor compartment. *J. Clin. Invest.* **67**, 673-680 (1981).

15. R.P. Eaton, N. Friedman, R.C. Allen, and D.S. Schade: Insulin removal in man: In vivo evidence for a receptor-mediated process. *J. Clin. Endocrinol. Metab.* **58**, 555-559 (1984).

16. G.T. Hammonds and L. Jarett: Lysosomal degradation of receptor-bound ^{125}I-labeled insulin by rat adipocytes. Its charcterization and dissociation from the short-term biologic

effects of insulin. *Diabetes* **29**, 475-486 (1980).

17. D.B. Donner: Receptor- and non-receptor-mediated uptake and degradation of insulin by hepatocytes. *Biochem. J.* **208**, 211-219 (1982).
18. J. Gliemann, O. Sonne, S. Linde, and B. Hansen: Biological potency and binding affinity of monoiodoinsulin with iodine in tyrosine A14 or A19. *Biochem. Biophys. Res. Com.* **87**, 1183-1190 (1979).
19. R.A. Pullen, D.G. Lindsay, S.P. Wood, I.J. Tickle, T.L. Blundell, A. Wollmer, G. Krail, D. Brandenburg, H. Zahn, J. Gilimann, and S. Gammeltoft: Receptor-binding region of insulin. *Nature* **259**, 369-373 (1976).
20. C.S. Cockram, R.H. Jones, A. Boroujerdi, and P.H. Sönken: Evidence for separate handling in vivo of different regions of the insulin molecule using A14- and B1-labeled insulin tracers. *Diabetes* **33**, 721-727 (1987).
21. G.R. Kingsley and G. Getchell: Direct ultramicro glucose oxidase method for determination of glucose in biologic fluids. *Clin. Chem.* **6**, 465-475 (1960).
22. A. Tsuji, T. Yoshikawa, K. Nishide, H. Minami, M. Kimura, E. Nakashima, T. Terasaki, E. Miyamoto, C.H. Nightingale, and T. Yamana: Physiologically based pharmacokinetic model for β-lactam antibiotics I: Tissue distribution and elimination in rats. *J. Pharm. Sci.* **72**, 1239-1251 (1983).
23. A. Tsuji, K. Nishide, H. Nimani, E. Nakashima, T. Terasaki, and T. Yamana: Physiologically based pharmacokinetic model for cefazolin in rabbits and its preliminary extrapolation to man. *Drug Metab. Dispos.* **13**, 729-739 (1985).
24. K. Yamaoka, T. Nakagawa, and T. Uno: Statistical moments in

pharmacokinetics. *J. Pharmacokin. Biopharm.* **6**, 547-558 (1978).

25. J.C. Sodoyez, F.R. Sodoyez-Goffaux, and Y.M. Moris: ^{125}I-insulin: kinetics of interaction with its receptors and rate of degradation in vivo. *Am. J. Physiol.* **239**, E3-E11 (1980).
26. H. Antoniades: Metabolism of single-component and high-molecular-weight radioactive insulin in rats. *Endocrinology* **99**, 481-489 (1976).
27. H.P.J. Bennett and C. McMartin: Peptide hormones and their analogues: Distribution, clearance from the circulation, and inactivation in vivo. *Pharmacol. Rev.* **30**, 247-292 (1979).
28. K. Yokono, R.A. Roth, and S. Baba: Identification of insulin-degrading enzyme on the surface of cultured human lymphocytes, rat hepatoma cells, and primary cultures of rat hapatocytes. *Endocrinology* **111**, 1102-1108 (1982).
29. P. De Meytes, A.R. Bianco, and J. Roth: Site-site interactions among insulin receptors. *J. Biol. Chem.* **251**, 1877-1888 (1976).
30. K. Siminoski, P. Gonnella, J. Bernanke, L. Owen, M. Neutra, R.A. Murphy: Uptake and transepithelial transport of nerve growth factor in suckling rat ileum. *J. Cell. Biol.* **103**, 1979-1990 (1986).
31. E.K. Frandsen and R.A. Bacchus: New, simple insulin-receptor assay with universal application to solubilized insulin receptors and receptors in broken and intact cells. *Diabetes* **36**, 335-340 (1987).

TABLE 1.

The total body clearance (CL_{tot}), steady-state volume of distribution (Vd_{ss}) of A_{14}-^{125}I-insulin and ^{14}C-inulin in mice

Tracer	CL_{tot} (ml/min/kg)	Vd_{ss} (ml/kg)
A_{14}-^{125}I-insulin		
Tracer dose (6.5 μCi/kg)	45.1 ± 3.1	1204 ± 195
+ unlabeled insulin (8 U/kg)	16.5 ± 0.4*	251 ± 13*
^{14}C-inulin (30 μCi/kg)	11.3 ± 1.5	181 ± 62

Using the plasma concentrations (n=3-5 for each data points) of A_{14}-^{125}I-insulin and ^{14}C-inulin after intravenous injection, CL_{tot} and Vd_{ss} were determined by a noncompartmental analysis as described in Materials and Methods, and are listed as mean ± a standard deviation (SD).

* Significantly different as compared with the value for tracer dose ($p<0.01$).

FIGURE LEGENDS

Fig. 1. *Representative HPLC elution profiles of A_{14}-^{125}I-insulin of the standard A_{14}-^{125}I-insulin (A), plasma (B) and tissue samples from kidney (C) and liver (D).*

Plasma and tissues were taken from mice 15 min after intravenous injection of A_{14}-^{125}I-insulin (6.5 μCi/kg). For the details of sample pretreatment see text. Open circles represent ^{125}I-radioactivity (cpm) in 1-ml fractions eluting from μ-Bondapak C_{18} column (Waters) with the acetonitrile gradient shown by a broken line. Flow rate was set at 1 ml/min. For other chromatographic conditions see text.

Fig. 2. *Relationship of intact percent of A_{14}-^{125}I-insulin between the TCA-precipitation and HPLC methods, obtained from plasma and tissue samples obtained at 5 min (▲), 15 min (Δ), 30 min (○) and 60 min (●) after iv injection in mice.*

After the pretreatment procedure, intact percent in each plasma or tissue sample (numbered as 1-17) was determined by both TCA-precipitation and HPLC. Note that TCA-precipitation consistently overestimates the intact percent of labeled insulin in biological samples as compared with HPLC.

Fig. 3. *Plasma disappearance curves of TCA-precipitable A_{14}-^{125}I-insulin (A) and HPLC-separated A_{14}-^{125}I-insulin (B) after intravenous bolus injection (6.5 μCi/kg) without (●) and with (○) a simultaneous injection of unlabeled insulin (8 U/kg) in mice.*

Disappearance of ^{14}C-inulin (30 μCi/kg) from plasma (▲) is also presented in panel C. Each point and vertical bar represent the mean ± SEM (n = 3-5).

Fig. 1

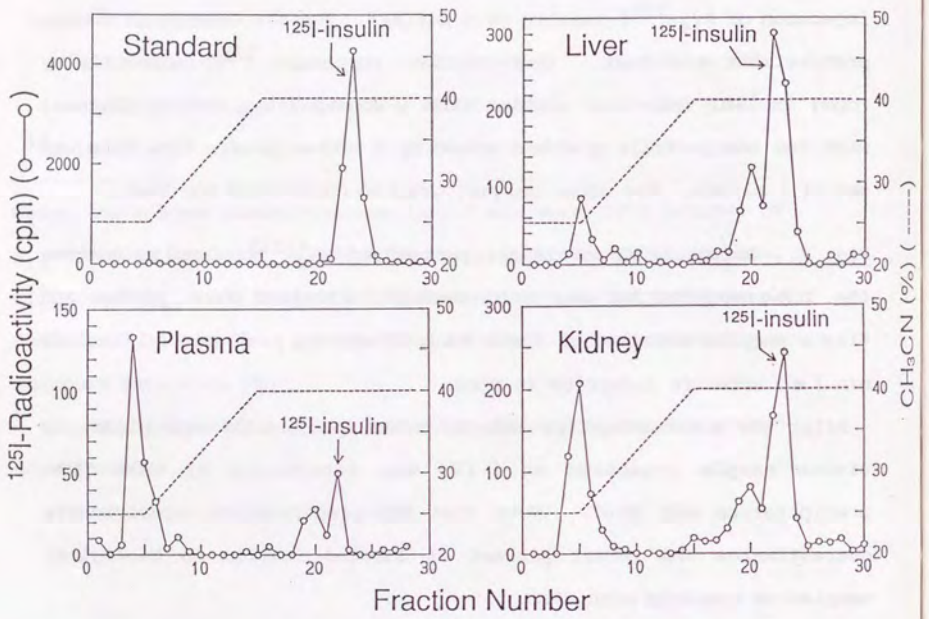
Standard
Liver
Plasma
Kidney
125I-insulin
125I-Radioactivity (cpm) (o—o)
CH3CN (%) (-----)
Fraction Number

Fig. 2

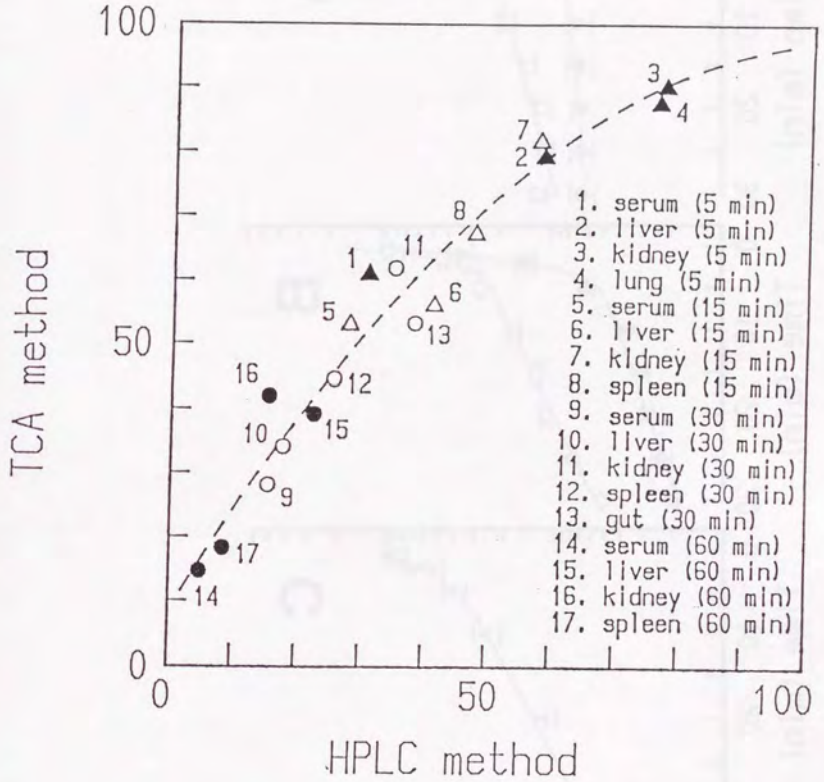
TCA method
HPLC method
1. serum (5 min)
2. liver (5 min)
3. kidney (5 min)
4. lung (5 min)
5. serum (15 min)
6. liver (15 min)
7. kidney (15 min)
8. spleen (15 min)
9. serum (30 min)
10. liver (30 min)
11. kidney (30 min)
12. spleen (30 min)
13. gut (30 min)
14. serum (60 min)
15. liver (60 min)
16. kidney (60 min)
17. spleen (60 min)

Fig. 3

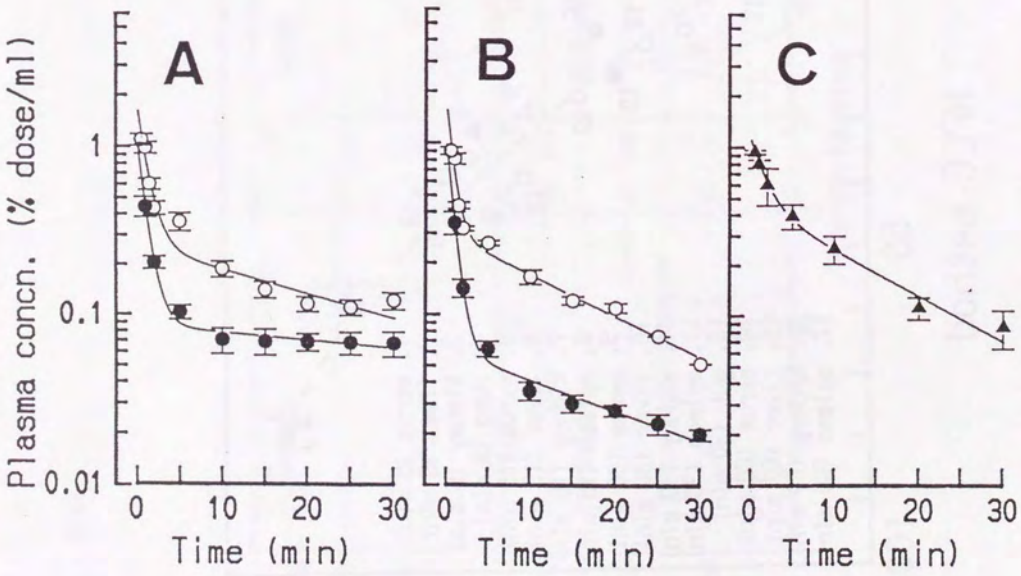

PART VII

EFFECT OF RECEPTOR UP-REGULATOIN ON INSULIN PHARMACOKINETICS IN STREPTOZOTOCIN-TREATED DIABETIC RATS

SUMMARY

The present study investigated the mechanism by which the disposition of insulin is altered in streptozotocin (STZ)-treated diabetic rats as compared with 48-hr fasted normal (control) rats. It was shown by an indocyanine green infusion method that the hepatic plasma flow rate (Q_H) in diabetic rats (1.64 ml/min/g liver) is significantly higher than that in control rats (0.982 ml/min/g liver). The portal injection technique revealed that the unidirectional clearance (CL_{on}), which represents the binding of A_{14}-^{125}I-insulin to surface receptors in the liver is significantly elevated in diabetic rats, suggesting an increase in the surface receptor number (R_T), i.e., up-regulation in the liver. In both control and diabetic rats, the total body clearance (CL_{tot}) and steady-state volume of distribution (Vd_{ss}) of labeled insulin decreased significantly with a simultaneous injection of unlabeled insulin (8 U/kg), confirming that the disposition of insulin is largely affected by specific, saturable receptor-mediated processes. The CL_{tot} and Vd_{ss} increased significantly in diabetic rats, while nonspecific portions of these parameters were not changed. From the increases in CL_{tot} (80%) and Q_H (67%) in diabetic rats, a pharmacokinetic analysis has revealed a 40% increase in the hepatic intrinsic clearance ($CL_{int,sp}$) of A_{14}-^{125}I-insulin *via* a specific mechanism in diabetic rats. In conclusion, we have provided *in vivo* evidence for a slight increase in $CL_{int,sp}$ of insulin in STZ-diabetic rats compared with control rats, which may be caused by an increase in the surface receptor number in the livers of diabetic rats.

INTRODUCTION

Diabetic mellitus is a chronic disorder characterized by a raised level of glucose in the blood. Streptozotocin (STZ) selectively destroys the pancreatic β-cell with production of permanent diabetes. Hypoinsulinemic diabetic animals, such as STZ-diabetic rats, have an increased binding capacity for insulin compared with control animals, due to an increased number of receptor sites on liver plasma membranes (1,2) and other target tissue membranes (3,4).

It has been recognized that an *in vivo* receptor compartment considerably affects insulin elimination and distribution (5-7). Philippe *et al.* (5) demonstrated that the metabolic clearance rate of ^{125}I-insulin was elevated in STZ-diabetic rats, and related this change to the increased binding of insulin to a specific receptor compartment. Moreover, using isolated liver perfusion experiments, Rabkin *et al.* (8) recently demonstrated that the hepatic clearance of immunoreactive insulin was significantly higher in hyperglycemic diabetic rats than that in control rats. In their study, the perfusion flow rate was set equal in control and diabetic groups. However, previous studies that compared insulin pharmacokinetics between normal and diabetic animals have disregarded a physiological change in blood flow rate, although hepatic clearance is dependent not only upon the intrinsic clearance activity but also upon the hepatic blood flow rate (9,10).

Moreover, it is known that insulin clearance is nonlinear and shows saturation at high physiologic insulin concentrations (11,12). Thus, when target tissues are exposed to different insulin concentrations in the entering blood, it is difficult to comprehensively compare the receptor number or intrinsic endocytotic activity between normal and

diabetic animals in *in vivo* conditions.

Therefore, the present study examined the changes in both the hepatic blood flow rates and portal insulin concentrations in control and STZ-diabetic rats, in order to provide a quantitative interpretation concerning the change in hepatic intrinsic clearance of insulin in a diabetic state.

MATERIALS AND METHODS

Chemicals. Human insulin ^{125}I-labeled at tyrosine-A_{14} (A_{14}-^{125}I-insulin), with a specific activity of 2,000 Ci/mmol, and ^{3}H-water, with a specific activity of 5 mCi/ml, were purchased from Amersham International Ltd. (Buckinghamshire, UK). Crystalline porcine insulin and bovine serum albumin (BSA, Fraction V) were obtained from Sigma Chemical Co. (St. Louis, MO), streptozotocin (STZ) and trichloroacetic acid (TCA) from Wako Pure Chemical Industries, Ltd. (Osaka, Japan), and indocyanine green (ICG) from Daiichi Pharmaceutical Co. (Tokyo, Japan). All other reagents were commercially available and of analytical grade. The monoiodinated insulin was dissolved in phosphate buffered saline (PBS) containing 0.1% BSA (designated as PBS solution) and stored at -20°C until study. The labeled insulin used was at least 98% pure as assayed by both TCA-precipitability and HPLC analysis. Distilled, deionized water was used throughout the experiments.

Animals. Male Wistar rats (200-230g) were obtained from Sankyo Laboratory Co., Ltd. (Toyama, Japan) and allowed free access to standard rodent chow and water. Control rats were fasted for 48 hr before experiments, while diabetic rats were not fasted.

Induction of Diabetes. Diabetes was induced by intravenous (i.v.) injection of a freshly prepared solution of STZ (65 mg/kg in saline/0.1 M citrate buffer, pH 4.5). Diabetic rats were studied 2 weeks after STZ injection. Control rats were untreated. Diabetes was recognized by reduced weight gain compared with control rats and by glycosuria (without ketonuria). Plasma glucose concentrations were measured by a glucose peroxidase method using a commercial kit (Glucose B-Test; Wako). Plasma insulin concentrations were determined

by radioimmunoassay using a commercial kit (IRI Eiken; Eiken Chemical Co., Ltd., Tokyo, Japan).

Determination of Hepatic Plasma Flow Rate. In control and diabetic rats, hepatic plasma flow rates (Q_H) were determined using an ICG infusion method. Briefly, under ketamine-xylazine anesthesia (ketamine, 235 mg/kg i.m.; xylazine, 2.3 mg/kg, i.m.), the abdomen was opened through a midline incision and the hepatic vein of the left lobe was cannulated according to the method of Yokota *et al.* (13) for the collection of hepatic venous blood. The left femoral vein and left femoral artery also were cannulated with SP-31 tubing. The abdomen was sutured after the correct cannulation was confirmed, and the rats were kept in the Bolman cages. A saline solution of ICG was infused into the femoral vein at the rates of 1.3μmol/hr and 0.86μmol/hr in control and diabetic rats, respectively, using an automatic infusion pump (model KN, Natsume Seisakusho Co., Tokyo, Japan). At designated times (0.5, 1, 1.5 and 2 hr), blood samples (0.25 ml) were withdrawn from the hepatic vein and femoral artery. Plasma was separated from blood by centrifugation, and the ICG concentration in plasma was determined as described later. Hematocrits (Ht) of the blood samples were measured using the last arterial and hepatic venous blood samples, and averaged. After the last blood samples were obtained, the whole liver was quickly excised, rinsed with saline, blotted dry on a filter paper, and weighed. The Q_H was determined as follows:

$$Q_H = IR/(Ca_{SS} - Cv_{SS}) \quad (1)$$

where IR is the infusion rate of ICG into the femoral vein, and Ca_{SS} and Cv_{SS} are the plasma ICG concentrations in the femoral arterial

plasma and hepatic venous plasma at steady-state, respectively.

Portal Vein Injection Technique. The unidirectional extraction of A_{14}-^{125}I-insulin in the liver was measured in control and diabetic rats, using the tissue sampling technique (14,15). Under ketamine-xylazine anesthesia, animals were placed in the supine position and laparotomized. After a portal vein was cannulated with a 27-gauge needle and the hepatic artery was ligated, an approximately 200-μl bolus of Ringer's-Hepes buffer (pH 7.4, 141 mM NaCl, 4 mM KCl, 2.8 mM $CaCl_2$, and 10 mM 4-(2-hydroxyethyl)-1-piperazineethansulfonic acid), containing 0.5μCi/ml A_{14}-^{125}I-insulin and 2.5μCi/ml ^{3}H-water with and without 50 μM unlabeled insulin, was rapidly injected within 0.5 sec into the portal vein. The ^{3}H-water was used as a highly diffusible internal reference of uptake. Eighteen seconds after portal injection, the portal vein was transected, and a portion of the right major lobe was immediately removed. The procedures of the sample treatment were the same as described previously (16). Briefly, aliquots of liver (~ 200 mg) and of the injection solution were counted in duplicate for simultaneous (^{125}I, ^{3}H) liquid scintillation counting according to the method described previously (17). The liver uptake index (LUI) was calculated as follows:

$$LUI\ (\%) = \frac{(^{125}I/^{3}H)\ \text{dpm in liver}}{(^{125}I/^{3}H)\ \text{dpm in injection solution}} \times 100 \quad (2)$$

The hepatic extraction of the test compound (E_T), A_{14}-^{125}I-insulin, was estimated from the following equation:

$$E_T = (LUI/100) \times E_R \quad (3)$$

where E_R is the percent extractions of the reference compound, ^{3}H-water, at 18 sec after rapid portal injection.

Determination of the Unidirectional Extraction of ^{3}H-Water. The operation procedures are the same as described above. A 200 µl-solution of ^{3}H-water (0.5µCi/ml) was injected and a portion of the right major lobe was immediately removed 18, 30, 45, 60 and 90 sec after portal injection. The unidirectional extraction of ^{3}H-water (E_R) was measured as follows:

$$E_R = (C_S/W_S)\ W_T/(C_I \cdot V_I) \quad (4)$$

where C_S and C_I are the ^{3}H-water radioactivity in the liver sample and injection solution (dpm/ml), respectively; W_S and W_T represent the liver weights (g) of the liver sample used for counting and the whole liver, respectively; and V_I is the total volume injected into the portal vein. The E_R at time t (min) can be expressed as follows:

$$E_R = E_{R,max}\ e^{-K_B t} \quad (5)$$

where $E_{R,max}$ and K_B represent the maximal (initial) extraction of the reference and the rate constant (min^{-1}) of ^{3}H-water efflux from the liver during a circulation period after portal injection, respectively. The K_B and E_{max} values were estimated by fitting the observed E_R data to Eq.(5), using a nonlinear least-squares regression analysis (18). These two parameters may be used to determine hepatic blood flow rate (F) using the following relationship:

$$F = \frac{K_B \cdot V'}{E_{R,max}} \quad (6)$$

where V' is the liver-blood partition coefficient for ^{3}H-water, which is 0.91 ml/g for the rat liver (15).

Intravenous Bolus Injection of A_{14}-^{125}I-insulin. Age-matched control and STZ-diabetic rats were lightly anesthetized with ether, and the femoral vein and left femoral artery were cannulated with polyethylene tubing (SP-31; o.d. 0.80 mm, i.d. 0.40 mm, Natsume Seisakusho) for

insulin administration and blood sampling, respectively. Before i.v. injection of A_{14}-^{125}I-insulin, control rats were kept in the Bolman cages and fasted for 48 hr for the monitoring of plasma concentrations of insulin and glucose. Diabetic rats were put into Bolman cages after the operation and stabilized for 1 hr. The control and diabetic conscious animals received an i.v. dose (3.2µCi/kg) of A_{14}-^{125}I-insulin with and without large excess of unlabeled insulin (8 U/kg), through the femoral vein. When unlabeled insulin was coadministered, glucose was constantly infused at a rate of 24 mg/min/kg to avoid hypoglycemia. Blood samples (approximately 0.3 ml) were withdrawn from the femoral artery at the designated times (2, 5, 10, 30, 60 and 120 min) after insulin administration and collected in polyethylene tubes. Serum was separated from blood by centrifugation, and the serum concentration of A_{14}-^{125}I-insulin was determined by TCA-precipitation and HPLC, as described later.

Analytical Methods. The ICG concentrations in plasma were measured spectrophotometrically at 800nm after 11 times dilution with water. A calibration curve was generated using plasma (from untreated rats) containing known quantities of ICG. Unchanged A_{14}-^{125}I-insulin in serum was measured by TCA-precipitation and HPLC analysis methods (7). Since it is very laborious to analyze many biological samples by HPLC, we routinely employed the TCA-precipitation method, and the obtained TCA-precipitability was converted into the percentage of unchanged A_{14}-^{125}I-insulin on HPLC, using a regression curve between these two methods.

Data Analysis.

1. The unidirectional clearance of insulin in the liver. Since a

portion of the unidirectional extraction represents simply distribution of label in the hepatic interstitial space, the hepatic extraction of A_{14}-^{125}I-insulin due to extravascular uptake, E_T', was calculated as follows:

$$E_T' = \frac{E_T - E_{suc}}{100 - E_{suc}} \quad (7)$$

where E_{suc} represents the apparent extracellular space in the liver, and taken as 13% (14). Thus, the unidirectional extraction of A_{14}-^{125}I-insulin due to "specific" binding to surface receptors ($E_{T,sp}'$) can be expressed as follows:

$$E_{T,sp}' = E_T' - E_{T,ns}' \quad (8)$$

where $E_{T,ns}'$ represents the unidirectional extraction of A_{14}-^{125}I-insulin due to "nonspecific" binding, which was calculated from LUI_{ns} in rats injected with a tracer plus unlabeled insulin. Then, the unidirectional clearance (CL_{on}) of A_{14}-^{125}I-insulin, which represents the association of insulin to surface receptors, was calculated based on well-stirred (Eq.(9)) and sinusoidal perfusion (Eq. (10)) models, as follows:

$$CL_{on} = \frac{Q_H \cdot E_{T,sp}'}{1 - E_{T,sp}'} \quad (9)$$

$$CL_{on} = -Q_H \cdot \ln(1 - E_{T,sp}') \quad (10)$$

2. Pharmacokinetic parameters of A_{14}-^{125}I-insulin. Serum concentrations (C) of A_{14}-^{125}I-insulin were expressed as percent of dose per ml serum as follows:

C = (total cpm/ml serum)x(intact percent in serum)/dose/100 (11)

where dose represents (intact cpm administered)/(kg body weight).

In control and diabetic rats, serum concentration *versus* time curves of A_{14}-^{125}I-insulin were analyzed by a noncompartmental moment method

(19) with an adequate extrapolation of observed data to infinite time, and the total body serum clearance (CL_{tot}) and steady-state apparent volume of distribution (Vd_{ss}) of A_{14}-^{125}I-insulin were calculated.

3. Hepatic intrinsic clearance of insulin due to a specific mechanism. Since the specific, receptor-mediated clearance of insulin can be attributed for the most part to the liver (6,8), the specific portion of CL_{tot} (named as $CL_{tot,sp}$) was assumed to be included in the hepatic clearance. Subsequently, the apparent hepatic intrinsic clearance of A_{14}-^{125}I-insulin ($CL_{int,sp,app}$) due to a specific mechanism was calculated, based on well-stirred (Eq. (12)) and sinusoidal perfusion (Eq. (13)) models, as follows:

$$CL_{int,sp} = \frac{Q_H \cdot CL_{tot,sp}}{Q_H - CL_{tot,sp}} \quad (12)$$

$$CL_{int,sp} = -Q_H \cdot \ln(1 - CL_{tot,sp}/Q_H) \quad (13)$$

where $CL_{tot,sp}$ represents the difference in CL_{tot} between the doses of a tracer alone and a tracer plus 8 U/kg of unlabeled insulin.

RESULTS

Characteristics of Animals. The body weight, plasma glucose, and insulin levels of the control and STZ-diabetic rats at time of the experiments are shown in Table I. Plasma glucose levels were significantly higher in STZ-diabetic rats than in control rats. Systemic insulin concentrations were low and very close between control and STZ-diabetic rats, while portal insulin concentrations were significantly higher in control rats.

Hepatic Plasma Flow Rate. As listed in Table II, hepatic plasma flow rate (Q_H) in STZ-diabetic rats (1.64 ml/min/g liver) was significantly higher than that in control rats (0.982 ml/min/g liver), while liver weight and hematocrit (Ht) were almost the same with each other.

Liver Uptake Index of A_{14}-^{125}I-insulin. The percent dose of ^{3}H-water extracted per g liver decreased monoexponentially (result not shown), and the obtained LUI parameters are listed in Table III. The CL_{on} was markedly elevated in STZ-diabetic rats compared with control rats, and the increase in CL_{on} was statistically significant, assuming that the E_R and F are constant in each group.

Pharmacokinetics of A_{14}-^{125}I-insulin. Since the relationship of A_{14}-^{125}I-insulin intactness (%) in serum samples between the TCA-precipitation and HPLC methods was essentially overlapping with that previously reported (7), the obtained TCA-precipitability, which was routinely employed for the determination of A_{14}-^{125}I-insulin in serum, was converted to the percentage of intact insulin on HPLC using their correlation. Serum disappearance curves of A_{14}-^{125}I-insulin in control and STZ-diabetic rats after i.v. injection are presented in Figs. 1A and 1B. The CL_{tot} and Vd_{ss} at a tracer dose were

significantly different between the control and STZ-diabetic rats, while those at a high dose were not significantly different. The CL_{tot} of A_{14}-^{125}I-insulin at a tracer dose (23.3 ml/min/kg) in control rats was in good agreement with that (23.6 ml/min/kg) reported previously in normal rats using ^{3}H-insulin as a tracer (20). In both groups of rats, the CL_{tot} and Vd_{ss} of labeled insulin decreased significantly with a simultaneous injection of unlabeled insulin (8 U/kg). Expressed in the unit of ml/min/g liver, the $CL_{tot,sp}$ and $CL_{int,sp}$ were elevated in diabetic rats by 46% and 40%, respectively. This is consistent with the study of Rabkin *et al.* (8), who observed 30% and 65% increases in the hepatic clearance (CL_H) and hepatic intrinsic clearance (CL_{int}) of immunoreactive insulin, respectively, in the perfused livers of diabetic rats. In this study, however, a statistical comparison of $CL_{tot,sp}$ or $CL_{int,sp}$ was not performed, because each parameter (i.e., Q_H and CL_{tot} at low and high doses) was determined in a different group of rats.

DISCUSSION

This study was designed to quantitatively evaluate the hepatic intrinsic clearance of insulin in diabetic states under an *in vivo* condition, where we have found a significant change in the hepatic plasma flow rate. Although the effect of hepatic blood flow rate on the elimination and distribution of drugs have been extensively studied (9,10,21), its effect on the hormone disposition has not been comprehensively understood due to the lack of quantitative analysis.

The portal injection technique revealed that CL_{on} is significantly higher in diabetic rats than in control rats (Table III). Since an intravenous injection of xylazine (0.5 mg) causes hypoinsulinemia for up to approximately 2 hr (22), the CL_{on} could be directly compared between control and diabetic rats without correction for the the extracellular insulin concentration (C_e), as described in the Appendix. It is generally considered that target cells from STZ-diabetic rats exhibit increased binding of ^{125}I-insulin, due to an increase in surface receptor number (R_T) with no change in receptor affinity (1-4). Thus, it is likely that the increased CL_{on} is attributed, for the most part, to an increase in the R_T. The present study, therefore, has provided *in vivo* evidence for the "up-regulation" of surface insulin receptors in the livers of STZ-diabetic rats.

With regard to the pharmacokinetic parameters of A_{14}-^{125}I-insulin (Table IV), the large Vd_{ss} at a tracer dose and its significant decrease with coadministration of unlabeled insulin suggest that insulin is not only distributed to the extracellular fluid but also reversibly bound to its specific binding sites (receptors) in target tissues. Moreover, the CL_{tot} was reduced significantly in control and

diabetic rats by 51% and 64%, respectively, with a simultaneous injection of unlabeled insulin. Taken altogether, it is confirmed that saturable and receptor-mediated processes of tissue distribution and elimination are involved in the pharmacokinetics of A_{14}-^{125}I-insulin in both groups of rats.

Philippe *et al.*(5) demonstrated that the metabolic clearance rate of ^{125}I-insulin was elevated by 44% in STZ-diabetic rats, and related this change to the increased binding of insulin to a specific receptor compartment in diabetic rats. However, since the previous study has not examined a change in hepatic blood flow rate or portal insulin concentrations, it has remained uncertain whether or not the hepatic intrinsic clearance (CL_{int}) of insulin was actually altered in STZ-diabetic rats. In this study, a significant increase in Q_H was observed in STZ-diabetic rats, despite the fact that the liver weight was not changed (Table II). This observation is consistent with previous reports demonstrating diabetes-induced increases in permeation of vessels and tissues by various tracer in diabetic humans and animals (23,24). On the other hand, the LUI method indicated that, under ketamine anesthesia, the hepatic blood flow rate (F) was 21% higher in diabetic rats than in control rats (Table III), and that these values were smaller than the hepatic blood flow rates measured with the ICG infusion, i.e., 1.89 and 3.03 ml/min/g liver in control and diabetic rats, calculated from $Q_H/(1 - Ht)$. This discrepancy could be explained by the effect of ketamine anesthesia on the hepatic blood flow rate, because Pardridge and Fiere (25) previously reported a 44% reduction of cerebral blood flow rate in the ketamine-anesthetized rats, as compared with conscious rats.

In addition to the hepatic plasma flow, we have to consider the difference in portal insulin concentration (C_p) between control and diabetic rats. In order to neglect such a difference, we attempted to minimize the C_p in control rats, so that an efficient hepatic extraction of insulin could be observed. McCarroll and Buchanan (26) reported mean extraction ratios of 22.2% for perfused livers of fed rats and 42.2% for preparations taken from fasted for 72 hr, supporting the view that the ability of the liver to extract insulin from the portal blood increases during fasting. Therefore, we used 48-hr fasted rats as control animal, in which the C_p was minimized but still higher than that in diabetic rats (Table I). When $CL_{int,sp}$ was corrected for the difference in C_p using Eqs. (A1)-(A5) in the Appendix, the $CL_{int,sp,corr}$ was shown to be higher in diabetic rats than in control rats by 24% and 31%, based on well-stirred and sinusoidal perfusion models, respectively. In any event, it is important to realize that an overall increase in CL_{tot} of A_{14}-^{125}I-insulin in STZ-diabetic rats could be interpreted as a result of the changes in not only $CL_{int,sp}$ and C_e but also Q_H (as a major factor).

In general, the $CL_{int,sp}$ can be expressed as follows:

$$CL_{int,sp} = k_{on} \cdot R_T \cdot k_e / (k_e + k_{off}) \qquad (14)$$

where k_e represents the endocytotic rate constant of insulin; k_{on} and k_{off} represent the association and dissociation rate constants of insulin-receptor binding, respectively. Eq.(14) indicates that an increase in R_T (or CL_{on}) and a decrease in k_e would affect $CL_{int,sp}$ (and also CL_{int}) in the opposite direction. Thus, the slight increase in $CL_{int,sp}$, which is inconsistent with the large increase in CL_{on}, might be accounted for by an decrease in k_e. This is a likely explanation, since there was a delay in the preclustering of

asialoorosomucoid receptors in the hepatocytes from diabetic rats (27). Therefore, further studies are required to clarify whether or not the k_e of insulin receptors is reduced in STZ-diabetic rats, using such as isolated hepatocytes.

In conclusion, from the significant increases in CL_{tot} and Q_H, we have provided *in vivo* evidence for a slight increase in $CL_{int,sp}$ of insulin in STZ-diabetic rats, which may be explained by counteracting effects of an increased surface receptor number (i.e., up-regulation) and an decreased endocytotic rate constant for insulin-receptor complex in the liver. Since the pharmacokinetic implications of physiological parameters (e.g., CL_{int}, Q_H and extracellular insulin concentration) appears to be lacking in the previous studies on insulin pharmacokinetics, the present study would be viewed as a physiological approach to the quantitative evaluation of receptor-mediated hepatic clearance of insulin.

Acknowledgements

The authors wish to thank Ms. Sekiko Yamada for her technical assistance. This study was supported by a Grant-in-Aid for Scientific Research from the Ministry of Education, Science and Culture of Japan, Project Research Fund from the Graduate School of Natural Science and Technology, Kanazawa University, and grants from the Nakatomi Foundation and Takeda Science Foundation.

APPENDIX

Equations to Calculate the Fraction of Unoccupied Surface Receptors in the Liver.

Considering the situation where the binding of extracellular insulin with surface receptors is in equilibrium, the fraction of unoccupied surface receptors (R) in the liver is given as follows:

$$R = 1 - C_e/(K_d + C_e) \quad \text{(A1)}$$

where K_d represents the dissociation constant of insulin-receptor binding, and C_e the average extracellular insulin concentration in the liver. Since the major portion of blood presented to the liver was from portal vein, the C_e can be approximately calculated using the well-stirred and sinusoidal perfusion models, as follows:

$$C_e \cong C_p\ (1 - E_H) \quad \text{(A2)}$$

$$C_e \cong -C_p \cdot E_H/\ln(1 - E_H) \quad \text{(A3)}$$

where C_p is the portal insulin concentration, and the hepatic extraction ratio (E_H) of insulin at steady state is obtained by:

$$E_H = Q_H/CL_H \quad \text{(A4)}$$

where Q_H and CL_H represent the hepatic plasma flow and hepatic insulin clearance, respectively. In this study, CL_H was taken as the specific portion of the total clearance, $CL_{tot,sp}$.

Since A_{14}-^{125}I-insulin is known to have the same receptor binding affinity with native insulin (29), and exhibits receptor binding to hepatocytes and isolated liver plasma membranes with a K_d of approximately 1 nM (30), we employed a representative K_d of 1 nM in Eq. (A1). Provided that an i.v. dose of A_{14}-^{125}I-insulin is so low that A_{14}-^{125}I-insulin could not interfere the binding of endogenous insulin to surface receptors in the liver, the hepatic intrinsic clearance of insulin ($CL_{int,sp}$) can be corrected for the difference in

C_e, as follows:

$$CL_{int,sp,corr} = CL_{int,sp}/R \quad \text{(A5)}$$

REFERENCES

1. M.B. Davidson and S.A. Kaplan. Increased insulin binding by hepatic plasma membranes from diabetic rats. *J. Clin. Invest.* **59**: 22-30 (1977).

2. R. Vigneri, N.B. Pilam, D.C. Cohen, V. Pezzino, K.Y. Wong, I.D. and Goldfine. In vivo regulation of cell surface and intracellular insulin binding sites by insulin. *J. Biol. Chem.* **253**: 8192-8197 (1978).

3. R. Rabkin, P. Hirayama, R.A. Roth and B.H. Frank. Effect of experimental diabetes on insulin binding by renal basolateral membranes. *Kidney Int.* **30**: 348-354 (1986).

4. M. Kobayashi and J.M. Olefsky. Effects of streptozotocin-induced diabetes on insulin binding, glucose transport, and intracellular glucose metabolism in isolated rat adipocytes. *Diabetes* **28**: 87-95 (1979).

5. J. Philippe, P.A. Halban and A. Gjinovci. Increased clearance and degradation of [^{3}H]insulin in streptozotocin diabetic rats. Role of the insulin-receptor compartment. *J. Clin. Invest.* **67**: 673-680 (1981).

6. J.C. Sodoyez, F.R. Sodoyez-Goffaux and Y.M. Moris. ^{125}I-insulin: Kinetics of interaction with its receptors and rate of degradatation in vivo. *Am. J. Physiol.* **239**: E3-E11 (1980).

7. H. Sato, A. Tsuji, K. Hirai and Y.S. Kang. Application of HPLC in disposition study of A14-^{125}I-labeled insulin in mice. *Diabetes* **39**: 563-569 (1990).

8. R. Rabkin, G.M. Reaven and C.E. Mondon. Insulin metabolism by liver, muscle, and kidneys from spontaneously diabetic rats. *Am. J. Physiol.* **250**: E530-E537 (1986).

9. G.R. Wilkinson and D.G. Shand. A physiological approach to hepatic drug clearance. *Clin. Pharmacol. Ther.* **18**: 377-390 (1975).

10. K.S. Pang and M. Rowland. Hepatic clearance of a drugs. I. Theoretical considerations of a 'well-stirred' model and a 'parallel tube' model. Influence of hepatic blood flow, plasma and blood cell binding, and the hepatocellular enzymatic activity on hepatic drug clearance. *J. Pharmacokin. Biopharm.* **5**: 625-653 (1977).

11. S. Fugleberg, K. Kølendorf, B. Thorsteinsson, H. Bliddal, B. Lund, F. and Bojsen. The relationship between plasma concentration and plasma disappearance rate of immunoreactive insulin in normal subjects. *Diabetologia* **22**: 437-440 (1982).

12. T. Morishima, C. Bradshaw and J. Radziuk. Measurement using tracers of steady-state turnover and metabolic clearance of insulin in dogs. *Am. J. Physiol.* **248**: E203-E208 (1985).

13. M. Yokota, T. Iga, S. Awazu and M. Hanano. Simple method of hepatic venous blood sampling in the rat. *J. Appl. Physiol.* **41**: 439-441 (1976).

14. W.M. Pardridge and L.S. Jefferson. Liver uptake of amino acids and carbohydrates during a single circulatory passage. *Am. J. Physiol.* **228**: 1155-1161 (1975).

15. W.M. Pardridge and L.J. Mietus. Transport of protein-bound steroid hormones into liver in vivo. *Am. J. Physiol.* **237**: E367-E372 (1979).

16. A. Tsuji, T. Terasaki, I. Tamai and K. Takeda. In vivo evidence for carrier-mediated uptake of β-lactam antibiotics through organic anion transport systems in rat kidney and liver. *J.*

Pharmaol. Exp. Ther. 253: 315-320 (1990).

17. T. Terasaki, K. Hirai, H. Sato, Y.S. Kang and A. Tsuji. Abosrptive-mediated endocytosis of a dynorphin-like analgesic peptide, E-2078, into the blood-brain barrier. *J. Pharmacol. Exp. Ther.* **251**: 351-357 (1989).
18. K. Yamaoka, Y. Tanigawara, T. Nakagawa and T. Uno. A pharmacokinetic analysis program (MULTI) for microcomputer. *J. Pharmacobio-Dyn.* **4**: 879-885 (1981).
19. K. Yamaoka, T. Nakagawa and T. Uno. Statistical moments in pharmacokinetics. *J. Pharmacobio-Dyn.* **6**: 547-558 (1978).
20. P.A. Halban, M. Berger and R.E. Offord. Distibution and metabolism of intravenously injected tritiated insulin in rats. *Metabolism* **28**: 1097-1104 (1979).
21. O. Nagata, M. Murata, H. Kato, T. Terasaki, H. Sato, A. and Tsuji. Physiological pharmacokinetics of a new muscle-relaxant, inaperisone, combined with its pharmacological effect on blood flow rate. *Drug Metab. Dispos.* **18**, 902-910 (1990).
22. S. López and B. Desbuquois. Insulin-related changes in the subcellular distribution of insulin receptors in intact rat liver: Effects of acute hypoinsulinemia induced by diazoxide, somatostatin, and xylazine. *Endocrinology* **120**: 1695-1702 (1987).
23. P. Kilzer, K. Chang, J. Marvel, E. Rowold, P. Jaudes, S. Ullensvang, C. Kilo and J.R. Williamson. Albumin permeation of new vessels is increased in diabetic rats. *Diabetes* **34**: 333-336 (1985).
24. J.R. Williamson, K. Chang, R.G. Tilton, C. Prater, J.R. Jeffrey, C. Weigel, W.R. Sherman, D.M. Eades and C. Kilo. Increased vascular permeability in spontaneously diabetic BB/W rats and in

rats with mild versus severe streptozotocin-induced diabetes. Prevention by aldose reductase inhibitors and castration. *Diabetes* **36**: 813-821 (1987).

25. W.M. Pardridge and G. Fierer. Blood-brain barrier transport of butanol and water relative to *N*-isopropyl-*p*-iodoamphetamine as the internal reference. *J. Cereb. Blood Flow Metabol.* **5**: 275-281 (1985).
26. A.M. McCarroll and K.D. Buchanan. Insulin clearance by the isolated perfused livers of insulin deficient rats. *Diabetologia* **9**: 457-460 (1973).
27. P. Scarmato, J. Feger, M. Dodeur, G. Durand and J. Agneray. Kinetic evidence of a surface membraneous step during the endocytosic process of ^{3}H-labelled asialoorosomucoid and its alteration in diabetic mellitus rats. *Biochim. Biophys. Acta* **843**: 8-14 (1985).
28. J.L. Carpentier, A. Robert, G. Grunberger, E.V. Obberghen, P. Freychet, L. Orci and P. Gorden. Receptor-mediated endocytosis of polypeptide hormones is a regulated process: Inhibition of [^{125}I]Iodoinsulin internalization in hypoinsulinemic diabetes of rat and man. *J. Clin. Endocrinol. Metab.* **63**: 151-155 (1986).
29. J. Gliemann, O. Sonne, S. Linde and B. Hansen. Biological potency and binding affinity of monoiodoinsulin with iodine in tyrosine A14 or tyrosine A19. *Biochem. Biophys. Res. Com.* **87**: 1183-1190 (1979).
30. D.A. Podlecki, B.H. Frank, M. Kao, H. Horikoshi, G. Freidenberg, S. Marshall, T. Ciaraldi and J.M. Olefsky. Characterization of the receptor binding properties of monoiodoinsulin isomers and

the identification of different insulin receptor specificities in hepatic and extrahepatic tissues. *Diabetes* 32: 697-704 (1983).

TABLE I.

Comparison of Body Weight, Plasma Glucose, and Plasma Insulin between Control and STZ-diabetic Rats[a]

Characteristics	Control	Diabetic
Body weight (g)	297 ± 5 (11)	176 ± 9* (5)
Plasma glucose (mg/dl)	149 ± 10 (7)	717 ± 22* (5)
Plasma insulin (pmol/l)		
Femoral vein	135 ± 15 (10)	147 ± 13 (4)
Portal vein	378 ± 18 (6)	179 ± 9 (4)*

[a] The data are expressed as the means ± SE. The numbers in parentheses represent the number of rats used.

* Significantly different from control rats ($p < 0.001$), as assessed by Student's *t*-test.

TABLE II.

Comparison of Hepatic Plasma Flow Rate, Liver Weight, and Hematocrit between Control and STZ-diabetic Rats[a]

Characteristics	Control	Diabetic
Hepatic plasma flow rate (ml/min/g liver)	0.982 ± 0.124	1.64 ± 0.05*
Liver weight (g)	10.5 ± 0.3	9.64 ± 0.60
Hematocrit (Ht)	0.480 ± 0.012	0.459 ± 0.010

[a] The data are expressed as the means ± SE from 3 rats.

* Significantly different from control rats ($p < 0.001$), as assessed by Student's *t*-test.

TABLE III.

Comparison of the LUI Parameters in Portal Injection Technique between Control and STZ-diabetic Rats

Compound	Parameter	Control	Diabetic
^{3}H-Water	$E_{R,max}$[a] (%)	73.2 ± 3.0	80.6 ± 11.5
	k_H[a] (min^{-1})	0.870 ± 0.069	1.21 ± 0.24
	F[b] (ml/min/g liver)	1.07	1.29
A_{14}-^{125}I-insulin[c]	LUI[d] (%)	145 ± 8	191 ± 10*
	LUI_{ns}[d] (%)	50.5 ± 4.0	54.9 ± 7.9
	E_T'[e] (%)	78.7 ± 5.2	96.3 ± 5.9
	$E_{T,ns}'$[e] (%)	17.6 ± 2.6	16.0 ± 4.5
	CL_{on}[f] (ml/min/g liver)		
	Well-stirred model	1.82 ± 0.38	5.56 ± 1.42*
	Sinusoidal perfusion model	1.03 ± 0.15	2.02 ± 0.34*

[a] Determined by Eq.(5) from a monoexponential decay curve of the ^{3}H-water extraction using a nonlinear least-squares regression analysis (18), and expressed as the mean ± SD.

[b] Calculated by Eq. (6), assuming that V' is 0.91 ml/g (15).

[c] The data are expressed as the mean ± SE. The numbers of rats used are 4 and 6 for control or diabetic rats, respectively.

[d] Calculated by Eq.(2).

[e] Calculated by Eq.(7).

[f] Calculated by Eqs.(9) and (10) for well-stirred and sinusoidal perfusion models, respectively.

* Significantly different from control rats ($p < 0.05$), as assessed by Student's *t*-test.

TABLE IV.

Comparison of Pharmacokinetic Parameters between Control and STZ-diabetic Rats[a]

Parameters	Dose	Control	Diabetic
CL_{tot}	tracer dose	23.3 ± 1.8 (6)	41.9 ± 8.5*(4)
(ml/min/kg)	+ unlabeled insulin	11.4 ± 0.5 (3)	14.9 ± 2.4 (3)
Vd_{ss}	tracer dose	1546 ± 68 (6)	2634 ± 352*(4)
(ml/kg)	+ unlabeled insulin	278 ± 18 (3)	399 ± 81 (3)
$CL_{tot,sp}$[b] (ml/min/kg)		11.9	27.0 (227%)[d]
(ml/min/g liver)		0.337	0.493 (146%)[d]
$CL_{int,sp}$[c] (ml/min/g liver)			
Well-stirred model		0.513	0.705 (137%)[d]
Sinusoidal perfusion model		0.408	0.585 (143%)[d]
$Vd_{ss,sp}$[b] (ml/kg)		1268	2235 (176%)[d]

[a] Using the serum concentrations of A_{14}-^{125}I-insulin after i.v. injection, the CL_{tot} and Vd_{ss} were determined by a noncompartmental moment analysis (19), and are expressed as mean ± SE. The numbers in parentheses represent the number of rats used.

[b] Determined as the difference of CL_{tot} or Vd_{ss} between the doses of a tracer only and a tracer plus 8 U/kg of unlabeled insulin.

[c] Determined by Eqs. (12) and (13) for well-stirred and sinusoidal perfusion models, respectively.

[d] The numbers in parentheses represent the ratio (%) of the parameters in STZ-diabetic rats to those in control rats.

* Significantly different from control rats ($p < 0.01$), as assessed by Student's *t*-test.

FIGURE LEGEND

Fig. 1. *Serum disappearance curves of A_{14}-^{125}I-insulin in control (panel A) and STZ-diabetic (panel B) rats after intravenous bolus injection (3.2μCi/kg) with (○) and without (●) 8 U/kg of unlabeled insulin.*

Each point and vertical bar represent the mean ± SE (n = 3-6). Solid lines were drawn by a nonlinear least-squares regression analysis (18) using a biexponential equation.

Fig. 1

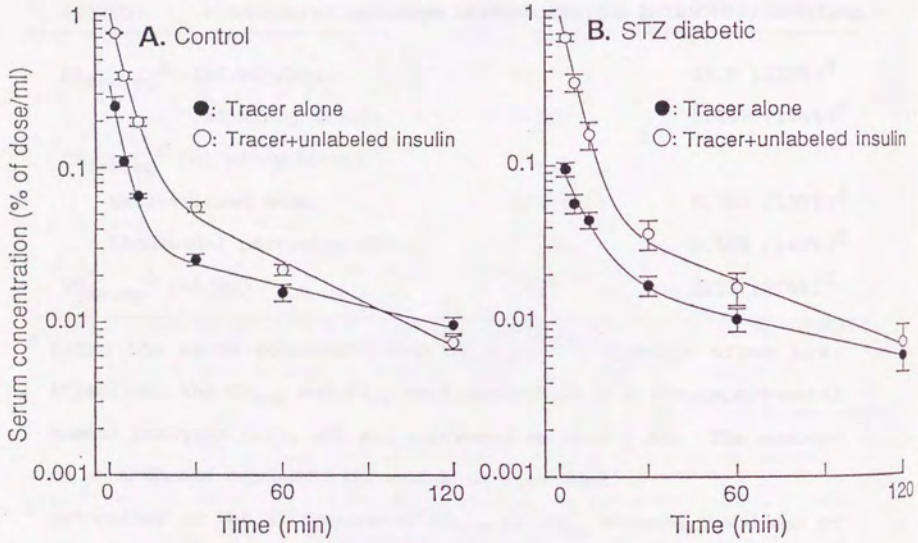
A. Control
B. STZ diabetic
●: Tracer alone
○: Tracer+unlabeled insulin
Serum concentration (% of dose/ml)
1
0.1
0.01
0.001
0
60
120
Time (min)

PART VIII

RECEPTOR-MEDIATED ENDOCYTOSIS OF A_{14}-^{125}I-INSULIN BY THE NONFILTERING PERFUSED RAT KIDNEY

SUUMMARY

The mechanism of insulin uptake and/or degradation in the peritubular circulation of the kidney was investigated using nonfiltering perfused rat kidneys, in which glomerular filtration was sufficiently reduced. After perfusion of A_{14}-^{125}I-insulin in the nonfiltering kidney for designated intervals, the acid-wash technique was employed to separately measure the acid-extractable and acid-resistant A_{14}-^{125}I-insulin, which were quantitated by HPLC and TCA-precipitability. HPLC profiles showed that the nonfiltering kidney metabolizes A_{14}-^{125}I-insulin only to a small extent during 1-hr perfusion, suggesting that the peritubular clearance of A_{14}-^{125}I-insulin was not due to extracellular degradation but for the most part to uptake by the kidney. Acid-extractable A_{14}-^{125}I-insulin rapidly increased with time and reached pseudo-equilibrium with perfusate at approximately 10 min, whereas acid-resistant A_{14}-^{125}I-insulin increased continuously. An endocytosis inhibitor, phenylarsine oxide, inhibited significantly the acid-resistant A_{14}-^{125}I-insulin with no change in acid-extractable A_{14}-^{125}I-insulin, suggesting that the peritubular uptake of A_{14}-^{125}I-insulin largely represents endocytosis of the peptide into the intracellular space. Moreover, both the acid-extractable and acid-resistant A_{14}-^{125}I-insulin were significantly decreased in the presence of unlabeled insulin (1 μM). These lines of evidence suggest that insulin is taken up by the nonfiltering perfused kidney *via* receptor-mediated endocytosis (RME), which possibly occurs at the basolateral side of renal tubular cells, and that the peritubular clearance of insulin is largely accounted for by this mechanism.

INTRODUCTION

Besides the liver, the kidney plays a major role in the clearance of insulin from the systemic circulation. This is supposed to be largely accounted for by glomerular filtration, and in part by postglomerular peritubular clearance [1]. Concerning a cellular mechanism of renal insulin degradation, Nielsen *et al.* [2] have suggested the existence of luminal and basolateral endocytosis of ^{125}I-insulin in isolated, perfused proximal tubules by the use of electron microscope autoradiography. Recently, Yagil *et al.* [3] have first provided direct evidence for the receptor-mediated endocytosis (RME) of ^{125}I-insulin from a luminal side of a cultured kidney cell line, in which a basolateral side has little or no direct exposure to the medium. Moreover, Dahl *et al.* [4] have shown that cultured epithelial cells exhibit a retroendocytotic pathway, i.e., exocytotic release of unchanged insulin after luminal endocytosis.

Insulin receptors have been identified in renal basolateral and brush-border membranes [5]. Hammerman [6] proposed that physiological actions of insulin in the renal proximal tubular cells are effected by binding of the hormone to specific receptors present in the basolateral membrane, followed by phosphorylation of these receptors. Consequently, it appears physiologically and biochemically important to investigate the interaction of insulin with its receptors and subsequent cellular events which might occur in the peritubular circulation in the kidney. Whiteside *et al.* [7] recently characterized the *in vivo* postglomerular interaction between ^{125}I-insulin and antiluminal surface of dog renal tubular cells by the use of a multiple indicator dilution (MID) technique. However, in their study, it was not clarified whether ^{125}I-insulin was transferred into

the intracellular space after binding to its receptors, since the MID technique cannot provide adequate information on relatively slow processes, such as endocytosis. Although the basolateral endocytosis of insulin in the renal tubules has been suggested *in vitro* [2], the mechanism involved in the peritubular clearance of insulin is obscure, due to the lack of direct evidence that A_{14}-^{125}I-insulin is transferred into the intracellular space *via* receptor-mediated or non-receptor-mediated endocytosis in the intact kidney.

Therefore, in the present study, we have provided kinetic evidence for the receptor-mediated endocytosis (RME) of A_{14}-^{125}I-insulin in the peritubular circulation, using the acid-wash technique [8,9] to discriminate between the surface-bound and internalized A_{14}-^{125}I-insulin, in the nonfiltering perfused rat kidney.

MATERIALS AND METHODS

Chemicals. Human insulin ^{125}I-labeled at tyrosine-A_{14} (A_{14}-^{125}I-insulin), with a specific activity of 2,000 Ci/mmol, was purchased from Amersham International Ltd. (Buckinghamshire, UK) and ^{3}H-inulin, with a specific activity of 500-1,000 mCi/mmol, from New England Nuclear Corp. (Boston, MA). Phenylarsine oxide (PhAsO), crystalline porcine insulin and bovine serum albumin (BSA, Fraction V) were obtained from Sigma Chemical Co. (St. Louis, MO), and trichloroacetic acid (TCA) and trifluoroacetic acid (TFA) from Wako Pure Chemical Industries, Ltd. (Osaka, Japan). Bovine erythrocytes were kindly supplied from the Meat Inspection Center of Kanazawa City (Ishikawa, Japan). All other reagents were commercially available and of analytical grade. The monoiodinated insulin was dissolved in phosphate buffered saline (PBS) containing 0.1% BSA (designated as PBS solution) and stored at -20°C until study. The labeled insulin used was at least 98% pure as assayed by both TCA-precipitability and HPLC. PhAsO was dissolved in dimethylsulfoxide (DMSO) and diluted 1000-fold into perfusion media before use. Distilled, deionized water was used throughout the experiments.

In Situ Kidney Perfusion. Adult male Wistar rats (Sankyo Laboratory Co., Ltd., Tokyo, Japan), weighing 280-350g and allowed free access to food and water, were anesthetized with intraperitoneal pentobarbital (50 mg/kg), and the right kidney was operated according to the method of Nishitsutsuji-Uwo *et al.* [10]. The perfusate consisted of 10% (vol/vol) washed bovine erythrocytes, 5% or 10% (wt/vol) BSA, 1 mg/ml glucose and a mixture of amino acids in Krebs-Henseleit bicarbonate (KHB) buffer (pH 7.4), as previously described [11]. Perfusate was continuously oxygenated by passage through a 7-m coil of Silastic

tubing (1.47 mm i.d., 1.96 mm o.d., Dow Corning Co., Midland, MI) contained in a glass box filled with 95% O_2-5% CO_2. Perfusate flow was monitored by a microflowmeter, and perfusate pressure at the inlet was monitored through a mercury manometer. After cannulations were completed, kidneys were perfused with erythrocyte-free KHB buffer in a single-pass system for 5 min, and perfused with 90 ml erythrocyte-containing KHB buffer in a closed-circuit system for 20-min stabilization until a tracer was added to the reservoir. Unless otherwise mentioned, the kidneys were maintained at 37°C by a warm plate attached to a temperature-adjustable heater and by perfusate flow, of which temperature at the inlet of the organ had been set at 37°C. Filtering kidneys were perfused with 5% BSA at an effective perfusion pressure of 98-105 mmHg and a constant flow rate of approximately 5.0 ml/min (including erythrocytes) using a peristaltic pump (model MP, Tokyo Rikakikai Co, Tokyo, Japan). In order to assess the degradation of A_{14}-^{125}I-insulin in the peritubular circulation and to examine whether insulin enters the cell through the basolateral membrane, nonfiltering perfused kidneys were utilized. Nonfiltering perfused kidneys were achieved by ligating the ureter and perfusing with the same perfusate containing a high perfusate BSA concentration (10%) at a slightly reduced perfusion pressure of 68-72 mmHg and a constant flow rate of approximately 4.5 ml/min (including erythrocytes), based on the method described previously [12].

Clearances of A_{14}-^{125}I-insulin and ^{3}H-inulin. For the determination of the renal clearances (CL_R) of A_{14}-^{125}I-insulin and ^{3}H-inulin in the filtering or nonfiltering perfused kidneys, each labeled compound was added to the reservoir at a tracer dose, i.e.,

approximately 0.30 μCi (1.7 pM in a final concentration) of A_{14}-^{125}I-insulin or 1.0 μCi of ^{3}H-inulin. Portions (500 μl) of the reservoir perfusate were sampled at appropriate times after the addition of a tracer, and centrifuged for 1 min in a microcentrifuge (Centrifuge 5412, Eppendorf GmbH, West Germany). A_{14}-^{125}I-insulin in perfusate samples (without erythrocytes) was assayed by either 5% trichloroacetic acid (TCA)-precipitability or HPLC as described later. The ^{3}H-radioactivity was determined in a liquid scintillation counter (model LSC-700, Aloka Co., Tokyo, Japan) using an external standard method for quenching correction.

In order to neglect differences in the dose of a tracer added to the perfusate, the concentrations of A_{14}-^{125}I-insulin and ^{3}H-inulin in the reservoir (Cp) were expressed as percentage of the initial perfusate concentration. In the case of A_{14}-^{125}I-insulin, Cp was calculated as unchanged insulin concentration, of which percentage unchanged was estimated from both TCA-precipitability and HPLC analysis. Since our pilot study showed that the concentrations of A_{14}-^{125}I-insulin and ^{3}H-inulin in the perfusate fell exponentially with time, the renal clearance (CL) of a tracer was calculated as:

$$CL = k\ V_p/KW \qquad (1)$$

where k is the exponential slope of the percent of initial concentration vs. time curve; V_p is the average perfusate volume (excluding erythrocytes) during the perfusion experiment; and KW is the kidney weight in grams.

Acid-Wash Technique in the Nonfiltering Perfused Kidney. At designated times after the addition of A_{14}-^{125}I-insulin at a dose of approximately 0.35 μCi (1.9 pM in a final concentration) into the reservoir, the kidneys were replaced in an open-circuit system and

briefly washed for 1 min with 10 ml of ice-cold saline for removing the unbound ^{125}I-radioactivity in the extracellular space and within the cannula. The kidneys were then perfused for 8 min with 40 ml of ice-cold KHB buffer, which had been adjusted to pH 3.0 by HCl (designated as acidic buffer). After four 10-ml fractions of acid-washout solution (designated as acid samples) containing acid-extractable ^{125}I-radioactivity were collected sequentially, whole kidneys were removed, weighed and homogenized in 4 ml of ice-cold 1 M acetic acid containing 6 M urea. The tissue homogenates containing acid-resistant ^{125}I-radioactivity were then centrifuged at 3,000 rpm for 15 min in a centrifuge (model RL-500SP, Tomy Seiko Co., Ltd., Tokyo, Japan) at 4°C, and the obtained supernatants (designated as tissue samples) were transferred to separate tubes for the assay of A_{14}-^{125}I-insulin. The percentage of ^{125}I-radioactivity recovered in the tissue samples was more than 90%.

Effects of Phenylarsine Oxide and Unlabeled Insulin. In order to examine the mechanism by which insulin is transported to a certain acid-resistant compartment, the following experiments were carried out. First, nonfiltering kidneys were perfused with A_{14}-^{125}I-insulin plus unlabeled insulin (1 μM) after 20-min preperfusion. Second, nonfiltering kidneys were pretreated for 20 min with 0.25 mM of PhAsO, an endocytosis inhibitor of proteins and polypeptides [13-15], before the addition of A_{14}-^{125}I-insulin. In both cases, acid-extractable and acid-resistant radioactivities of A_{14}-^{125}I-insulin were determined by the above-mentioned acid-wash technique after 30-min perfusion.

Analytical Methods. TCA-precipitation and HPLC analysis were employed according to the methods described previously [16], in order

to estimate the intactness of A_{14}-^{125}I-insulin in the reservoir perfusates, acidic perfusates and tissue homogenates.

TCA-Precipitation. Perfusate samples (300 μl) were mixed well with an equal volume of 10% (wt/vol) TCA solution, while acid samples (1 ml) or tissue samples (1 ml) with a fifth volume of 30% (vol/vol) TCA solution, to give a final TCA concentration of 5%. These mixtures were kept standing at 4°C for 30 min, centrifuged at 3,000 x *g* for 15 min, and the supernatants were transferred into separate tubes by aspiration. The ^{125}I-radioactivity in the precipitates and supernatants was measured in a γ-counter (model ARC-605, Aloka Co.). The percentage of radioactivity precipitable by TCA was calculated as (cpm in precipitate)/[(cpm in precipitate) + (cpm in supernatant)] x 100, and taken as the percentage of unchanged A_{14}-^{125}I-insulin estimated by the TCA-precipitation method.

HPLC Analysis. Perfusates (300 μl) and tissue samples (1 ml) were deproteinized by mixing vigorously with an equal volume of ethanol, and centrifuged at 10,000 x *g* for 5 min in a microcentrifuge (MR-15A, Tomy Seiko Co.). Ethanol-treated supernatants from the tissue samples, as well as the first 10-ml fraction of acid samples, were lyophilized and reconstituted in a mixture of acetonitrile and water (50:50, vol/vol) containing 0.1 % (vol/vol) TFA. The ethanol-treated supernatants of the perfusate samples and the reconstituted samples of tissue and acid samples were filtered through 0.45-μm millipore filters (type HV; Nihon Millipore Kogyo, Yonezawa, Japan) with the recovery of more than 80%, and resultant filtrates (100 μl) were loaded onto a reversed-phase HPLC column, μ-Bondapak C_{18} (30 cm x 3.9 mm i.d., Waters Associates, Inc., Milford, MA). The solvent delivery system, LC-6A (Shimadzu Corp., Kyoto, Japan) was equipped with an

ultraviolet detector, SPO-6A (Shimadzu Corp.) and a gradient programmer, SCL-6A (Shimadzu Corp.). A guard column, C_{18} CORASIL (Waters Associates, Inc.) was placed between the injector and the analytical column. The mobile phase consisted of two solvents: solvent A was water containing 0.1% (vol/vol) TFA; and solvent B a mixture of acetonitrile and water (50:50, vol/vol) containing 0.1% (vol/vol) TFA. After an isocratic run at 50% solvent B for 5 min, a linear gradient was run from 50% to 80% solvent B for 15 min, and 80% solvent B was held for 10 min. The solvent flow rate was 1.0 ml/min, and the column and solvents were kept at room temperature. The column used was standardized with 3-I-L-tyrosine, A_{14}-^{125}I-insulin and unlabeled porcine insulin. The eluents were collected automatically and the radioactivity in each fraction (0.8 ml) was counted using a γ-counter. The percentage of ^{125}I-radioactivity associated with intact A_{14}-^{125}I-insulin was calculated by measuring the peak areas eluted from the column. The total radioactivity eluted from the column was almost 100% of the radioactivity loaded onto the column.

RESULTS

In Situ Kidney Perfusion. Using the isolated basolateral membranes prepared from rat renal cortex [17] of which purity was described previously [18], the specific binding of A_{14}-^{125}I-insulin to the basolateral membranes was determined to be 86.7% of the total binding, indicating that the use of this labeled peptide is adequate to analyze the interaction with its receptors in the peritubular circulation. A_{14}-^{125}I-insulin was perfused in the perfusion apparatus without the kidney and no loss of the ^{125}I-radioactivity from the reservoir was observed, indicating that the clearance of A_{14}-^{125}I-insulin from the reservoir was not due to adsorption of A_{14}-^{125}I-insulin to the perfusion apparatus, but to the clearance by the filtering or nonfiltering kidney.

Table I summarizes the characteristics of the filtering and nonfiltering perfused rat kidneys employed in this study. Perfusate plasma flow rate was set close to *in vivo* renal plasma flow (RPF), and 10% erythrocytes were added to the perfusate to avoid the renal ischemia. In the filtering kidney, the kidney function was shown to be normal and constant in terms of the perfusate flow rate, perfusion pressure, and urine flow rate, and GFR was consistent with that (0.44 ml/min/kidney) reported previously [19]. In the nonfiltering perfused kidneys, GFR was sufficiently reduced, whereas the changes in the renal perfusate flow rate and perfusion pressure were minimal, and the metabolic integrity of the renal tissue was reportedly preserved [11].

Figures 1A and 1B show typical HPLC profiles of ^{125}I-radioactivity collected from the reservoir perfusate after 0-min (panel A) and 60-min (panel B) perfusion of A_{14}-^{125}I-insulin in the recirculating mode

of the nonfiltering perfused kidneys. As can be clearly seen, approximately 85% of the ^{125}I-radioactivity in the perfusate coeluted with A_{14}-^{125}I-insulin (retention time, 21 min) as a single sharp peak, and the peaks of A_{14}-^{125}I-insulin eluted from these samples are almost identical, indicating that the nonfiltering kidney could metabolize A_{14}-^{125}I-insulin only to a small extent during 1-hr perfusion. This is consistent with a previous report by Duckworth *et al.* [20] that only 10.6% of the insulin-sized material was not intact insulin in perfusate from a nonfiltering kidney. A small peak eluting at 3-4 min probably represents a mixture of $^{125}I^-$ and monoiodotyrosine, because a standard 3-I-L-tyrosine eluted as early as 3.9 min and very close to the salt peak (3.1 min) under the present analytical condition. The identity of a small peak eluting at 16 min is not clear from the present study, but it possibly represents intermediate degradation products of labeled insulin, because previous HPLC studies have demonstrated TCA-precipitable, insulin-sized intermediate products derived from enzymatic interactions of insulin with various tissues, such as adipocytes [21] and hepatocytes [22].

Acid-Wash Technique in the Nonfiltering Perfused Kidney. When a kidney was washed with 10-ml of ice-cold saline and then with 40-ml of ice-cold acidic buffer at 4°C, two sharp peaks of ^{125}I-radioactivity were sequentially eluted from the kidney through the outflow cannula (results not shown). The radioactivity in the cannulas after saline-wash and acid-wash was measured occasionally, and found to be in the background level. Therefore, the observed acid-extractable radioactivity could not be attributed to the adsorption of A_{14}-^{125}I-insulin or of its degradation products within the cannulas, but to the

release from an acid-sensitive compartment in the kidney.

Figures 2A and 2B show typical HPLC profiles of the acid-extractable and acid-resistant ^{125}I-radioactivity, respectively, after 60-min perfusion of A_{14}-^{125}I-insulin in the nonfiltering perfused kidneys. More than 60% of the ^{125}I-radioactivity in these samples coeluted with A_{14}-^{125}I-insulin as a single sharp peak, suggesting that insulin transferred into the acid-resistant compartment was not so unstable at least for 60 min. Since the percentage of intact A_{14}-^{125}I-insulin on HPLC was very close to TCA-precipitability in these samples, the TCA-precipitation method was routinely employed thereafter.

Figure 3 shows the time-dependent changes of the acid-extractable A_{14}-^{125}I-insulin, acid-resistant A_{14}-^{125}I-insulin, and acid-resistant degradation products of A_{14}-^{125}I-insulin, in the nonfiltering perfused kidneys. Obviously, the acid-extractable A_{14}-^{125}I-insulin rapidly increased with time and reached pseudo-equilibrium with the perfusate at approximately 10 min, whereas the acid-resistant A_{14}-^{125}I-insulin increased in a linear fashion over the time-interval examined. By contrast, acid-resistant degradation products of A_{14}-^{125}I-insulin in the kidney fell considerably less than the acid-resistant A_{14}-^{125}I-insulin, with a slight increase with time.

Internalization and degradation of A_{14}-^{125}I-insulin in the nonfiltering perfused kidney were analyzed according to the method previously employed for the RME of insulin [13] and epidermal growth factor (EGF) in hepatocytes [23]. As formulated in the Appendix, this kinetic analysis is based on differential equations describing the time-dependent changes in the amounts (cpm) of the surface-bound insulin (X_s), internalized insulin (X_{in}) and intracellular degradation

products of insulin (X_{deg}). Since X_s was almost constant and X_{in} increased linearly with time during 10-60 min (Fig. 3), the endocytotic rate constant (k_{end}) was determined to be 0.022 min^{-1} using Eqn. (A5) as described in the Appendix. The obtained value of k_{end} falls between the reported k_{end} values obtained in rat hepatocytes (0.12 min^{-1}) [24] and myocytes (0.0018 min^{-1}) [25], suggesting that the rate of endocytosis is closely related with physiological significance of receptor internalization in various tissues (e.g., regulation of the responsiveness to the hormone, inactivation of the hormone, and intracellular signaling after RME).

Effects of Phenylarsine Oxide and Unlabeled Insulin. As shown in Fig. 4, PhAsO (250 μM) inhibited significantly the acid-resistant A_{14}-^{125}I-insulin, with no change in the acid-extractable A_{14}-^{125}I-insulin. Moreover, as shown in Fig. 5, both the acid-extractable and acid-resistant A_{14}-^{125}I-insulin were significantly decreased in the presence of unlabeled insulin (1 μM).

DISCUSSION

This study was designed to provide kinetic evidence for the RME of insulin in the nonfiltering perfused kidney. Most of the previous studies on renal handling of insulin using isolated kidneys have been performed using the perfusion flow rates 4-10 times higher than the physiological RPF, to supply enough oxygen to maintain the kidney function. However, the organ clearance is dependent upon the blood flow rate [26] and there might be some difference in the dependence of GFR and peritubular clearance of insulin on RPF. Therefore, in the present study, we included 10% bovine erythrocytes in the perfusate as an oxygen carrier at the perfusion flow rate (4.4 ml/min/g kidney) close to that of normal RPF in rats (3.7 ml/min/g kidney) [27], so that we could provide a better insight into the mechanism of renal peritubular clearance under the physiological condition without possible artificial factors.

The protein binding of A_{14}-^{125}I-insulin in the perfusate was examined by the polyethylene glycol precipitation method [28], and determined to be negligible in KHB buffer containing 5% or 10% BSA (results not shown). Accordingly, provided that the sieving coefficient of unbound insulin is identical with that of inulin at the glomeruli, the peritubular clearance of A_{14}-^{125}I-insulin can be calculated as simply a difference between the renal clearance of A_{14}-^{125}I-insulin and that of inulin in the filtering kidney (0.052 ml/min/g kidney). Thus, the peritubular clearance accounts for 11% of the overall renal clearance of insulin. Moreover, the present study indicates that the insulin clearance by the nonfiltering kidney is approximately 30% of that by the filtering kidney (Table 1), and that the peritubular insulin clearance by the nonfiltering kidney is

slightly larger than that by the filtering kidney. This is consistent with the inverse correlation between GFR and peritubular clearance of immunoreactive insulin, reported by Rabkin and Kitabchi [19], although the large difference in the renal perfusion flow rate between the present study (4.0-4.4 ml/min) and previous studies (25-50 ml/min) [12,19,29-31] makes it difficult to compare directly the insulin clearance values between this study and others. Moreover, our results on the peritubular insulin clearance are consistent with the report by Peterson *et al.* [12], who observed that the peritubular insulin clearance is 17% of the total renal clearance in the filtering kidney, and that the insulin clearance by the nonfiltering kidney is 47% of that by the nonfiltering kidney. Taken all together, our kidney perfusion system appears to be a suitable model to investigate the mechanism of peritubular clearance of insulin.

There have been controversial reports concerning the peritubular insulin clearance by the nonfiltering kidney, the discrepancy being obscure. For example, Maude *et al.* [30] observed that the renal clearance of insulin was not changed when GFR is sufficiently reduced, and suggested that the peritubular insulin clearance increases considerably in order to compensate for the decrease in insulin delivery to the luminal face of the tubular cells. On the other hand, Schlatter *et al.* [31] observed that peritubular uptakes of pig- and rat-insulins accounted for 13% and 31% of the total renal clearance, respectively, but that the nonfiltering kidney does not remove insulin from the peritubular circulation. They concluded that the filtration process seems to be necessary for the uptake of insulin at the peritubular site. We prefer the interpretation that the above-

mentioned discrepancy is due to differences in the affinity of the tracer and in assay methods, as well as differences in experimental conditions (e.g., endogenous insulin level), which have made it difficult to comprehensively integrate much information on insulin pharmacokinetics reported previously from different laboratories. This is why we chose HPLC-purified A_{14}-^{125}I-insulin as a tracer, which is known to be indistinguishable from native insulin in its recetor binding property and biological potency [32,33], and employed an HPLC analysis to evaluate the insulin-sized, intermediate degradation products of inuslin [16,20-22].

As also inspected from Figs. 1A and 1B, the ^{125}I-radioactivity associated with intact A_{14}-^{125}I-insulin in the perfusate samples at 0 min was not reduced after 1-hr perfusion, with no increase in the intermediate products. These results on HPLC are consistent with no change in TCA-precipitability in the same samples (i.e., 96% and 95%, before and after 1-hr perfusion, respectively). The negligible degradation of A_{14}-^{125}I-insulin in the perfusate from the nonfiltering kidney suggests that the peritubular clearance of A_{14}-^{125}I-insulin is not attributed to degradation but to uptake at some place facing the peritubular circulation. Interestingly, the slow degradation of insulin in the nonfiltering kidney is compatible with a proposal by Rabkin *et al.* [29] that peritubular uptake of insulin lacks the feature of a process involving lysosomal degradation, although the exact itinerary of insulin endocytosed from this side is uncertain at present. The peritubular capillaries are closely juxtaposed to the basolateral membranes of the tubular cells. These highly permeable fenestrated capillaries supply the tubular cells with not only O_2 and small solutes (i.e., nutrients) but also large-molecular-weight

compounds < 6,000 dalton [34], in the size range of insulin. Moreover, Whiteside *et al.* [7] applied the MID method to investigate the kinetic behaviors of insulin in the peritubular circulation, and their computer-assisted model analysis suggested no saturable interaction of ^{125}I-insulin with the "endothelium". Therefore, it is reasonable to assume that the transfer of A_{14}-^{125}I-insulin into an acid-resistant compartment occurs at the basolateral face of peritubular circulation in the nonfiltering perfused kidney, i.e., at the basolateral side of renal tubular cells. Indeed, binding and degradation of insulin by the glomerular capillaries and peritubular vessels could account, in part, for insulin removal by the nonfiltering kidney, but it is likely that most of the insulin binds to receptors located on the peritubular surface of the tubular cells.

It is known that the binding of insulin with its receptor could be sufficiently dissociable at low pH [35]. Previous studies have confirmed the efficacy of the acid-wash technique in isolated hepatocytes [13]. In the present study, the time-dependent increase of the acid-resistant A_{14}-^{125}I-insulin (Fig. 3), together with the effects of PhAsO and unlabeled insulin on the acid-resistant and acid-extractable A_{14}-^{125}I-insulin (Figs. 4 and 5), suggest that the observed acid-resistant A_{14}-^{125}I-insulin largely represents the intracellular A_{14}-^{125}I-insulin taken up by a saturable endocytotic process, that is, RME.

RME is a process in which the receptor-ligand complex is internalized into the intracellular space. The initial perfusate concentration of A_{14}-^{125}I-insulin employed was so low (1.9 pM) that the receptor occupation in the tubular cells by insulin should be very

small. Thus, the number of surface receptors could not be affected by the internalization of receptors with the tracer concentration of A_{14}-^{125}I-insulin, resulting in the continuous, linear increase of acid-resistant A_{14}-^{125}I-insulin. This is compatible with no change of the acid-extractable A_{14}-^{125}I-insulin in the presence of PhAsO, while the acid-resistant A_{14}-^{125}I-insulin was significantly decreased. Besides the internalization of receptors occupied by a ligand, it is also known that "unoccupied receptors" are spontaneously internalized at a slower rate [25,36]. However, the k_{end} value obtained here represents the endocytotic rate constant of "occupied receptors", because the endocytotic process was measured with surface-bound and internalized A_{14}-^{125}I-insulin, but not with receptor movement itself.

Although Maratos-Flier *et al.* [37] reported that there was no transport of insulin in either apical-to-basal or basal-to-apical direction in the Madin-Darby canine kidney (MDCK) cells, it does not necessarily mean that there was no endocytosis of insulin in either direction across the renal epithelial cells. In fact, there are some evidence for luminal endocytosis and apical-to-basal transcytosis of insulin provided using cultured epithelial cells or proximal tubules [2-4], whereas there is little direct evidence for basolateral endocytosis. In the present study, GFR was not completely diminished in the nonfiltering kidney (Table I), casting a doubt that the observed internalization of A_{14}-^{125}I-insulin might be a consequence of luminal endocytosis rather than that of basolateral endocytosis. In contrast to the small degradation of A_{14}-^{125}I-insulin observed in the nonfiltering kidney (Figs. 1 and 2), Herrman *et al.* [38] have reported that approximately 85% of the radioactivity in the 1-hr perfusate was in the form of low-molecular-weight products in the filtering kidney,

as assayed by gel filtration chromatography. Therefore, the internalized A_{14}-^{125}I-insulin (Fig. 2B) should have been more extensively degraded, if A_{14}-^{125}I-insulin was taken up more from the luminal side than from the basolateral side.

Nielsen and Christensen [39] have shown that there is a small but significant basolateral endocytotic uptake of both cationized ferritin and horseradish peroxidase (HRP) in a preparation of perfused proximal tubules, in which erroneous interpretations due to luminal uptake were excluded. They have also suggested that proteins taken up from the peritubular side are transferred not only to lysosomes but also to multivesicular bodies. In this study, 80% inhibition of the endocytosis of A_{14}-^{125}I-insulin was observed in the presence of 1 μM unlabeled insulin, but its inhibition was not complete (Fig. 5). Therefore, we cannot exclude the possibility that a nonselective endocytosis contributes, at least in part, to the internalization of insulin from the basolateral side of the renal tubular cells. Thus, further study should be focused on the specificity of the basolateral endocytosis and the intracellular itinerary of internalized insulin.

In conclusion, we have provided kinetic evidence for the RME of A_{14}-^{125}I-insulin in the nonfiltering perfused rat kidney, which possibly occurs at the basolateral side of renal tubular cells. It was also suggested that the peritubular clearance of insulin is largely accounted for by this mechanism.

Acknowledgments

This study was supported by a Grant-in-Aid for Scientific Research from the Ministry of Education, Science and Culture of Japan, Project Research Fund from the Graduate School of Natural Science and Technology, Kanazawa University, and grants from Takeda Science Foundation and Nakatomi Foundation. The authors thank Mr. Saburo Okabe, the Meat Inspection Center of Kanazawa City, for graciously providing us with fresh bovine erythrocytes.

APPENDIX

Kinetic Analysis for Receptor-Mediated Endocytosis (RME) of Insulin.

The binding of a ligand to its cell surface receptor is the first step in RME. The pool of occupied surface receptors can thus be regarded as the substrate of endocytosis. Given the general case in which the internalization process is first order with respect to the occupied receptors, then the change in intracellular ligand (X_{in}) can be described as:

$$\frac{dX_{in}}{dt} = k_{end} \cdot X_s - k_{deg} \cdot X_{in} \qquad (A1)$$

where X_s, k_{end} and k_{deg} represent the amounts of surface-bound A_{14}-^{125}I-insulin (cpm), endocytotic rate constant (min^{-1}) for the surface-bound ligand and degradation rate constant (min^{-1}) for the intracellular ligand, respectively. Moreover, it is assumed that the increase of intracellular degradation products (X_{deg}) can be described as:

$$\frac{dX_{deg}}{dt} = k_{deg} \cdot X_{in} - k_{rel} \cdot X_{deg} \qquad (A2)$$

where k_{rel} represents the releasing rate constant (min^{-1}) for intracellular degradation products of the ligand, respectively. Summation of both side hands of Eqns. (A1) and (A2) yields:

$$\frac{dX_{in}}{dt} + \frac{dX_{deg}}{dt} = k_{end} \cdot X_s - k_{rel} \cdot X_{deg} \qquad (A3)$$

During the intracellular degradation products (X_{deg}) are not yet released substantially (i.e., $X_s > X_{deg}$ and $k_{end} > k_{rel}$), Eqn. (A3) can be approximated to:

$$\frac{d(X_{in} + X_{deg})}{dt} = k_{end} \cdot X_s \qquad (A4)$$

Finite integration of Eqn. (A4) from $t = t_1$ to $t = t_2$ at steady-state (i.e., X_s is constant) gives:

$$k_{end} = \frac{\Delta(X_{in} + X_{deg})}{X_s \Delta t} \qquad (A5)$$

Thus, k_{end} can be estimated from the observed values of surface-bound ligand and internalized ^{125}I-radioactivity.

REFERENCES

1. R. Rabkin, M.P. Ryan, and W.C. Duckworth: The renal metabolism of insulin. *Diabetologia* **27**, 351-357 (1984).

2. S. Nielsen, J.T. Nielsen, and E.I. Christensen: Luminal and basolateral uptake of insulin in isolated, perfused, proximal tubules. *Am. J. Physiol.* **253**, F857-F867 (1987).

3. C. Yagil, U.K. Ehmann, B.H. Frank, and R. Rabkin: Insulin binding, internalization, and degradation by a cultured kidney cell line. *Am. J. Physiol.* **254**, E601-E608 (1988).

4. D.C. Dahl, T. Tsao, W.C. Duckworth, M.J. Mahoney, and R. Rabkin: Retroendocytosis of insulin in a cultured kidney epithelial cell line. *Am. J. Physiol.* **257**, C190-C196 (1989).

5. Z. Taylor, D.S. Emmanouel, and A.I Katz: Insulin binding and degradation by luminal and basolateral tubular membranes from rabbit kidney. *J. Clin. Invest.* **69**, 1136-1146 (1982).

6. M.R. Hammerman: Interaction of insulin with the renal proximal tubular cell. *Am. J. Physiol.* **249**, F1-F11 (1985).

7. C.I. Whiteside, C.J. Lumsden, and M. Silverman: In vivo characterization of insulin uptake by dog renal cortical epithelium. *Am. J. Physiol.* **255**, E357-E365 (1988).

8. W.A. Dunn and A.L. Hubbard: Receptor-mediated endocytosis of epidermal growth factor by hepatocytes in the perfused rat liver: Ligand and receptor dynamics. *J. Cell Biol.* **98**, 2148-2159 (1984).

9. M. Suzuki, F.A. Almeida, D.R. Nussenzveig, D. Sawyer, and T. Maack: Binding and functional effects of atrial natriuretic factor in isolated rat kidney. *Am. J. Physiol.* **253**, F917-928 (1987).

10. J.M. Nishitsutsuji-Uwo, B.D. Ross, and H.A. Krebs: Metabolic activities of the isolated perfused rat kidney. *Biochem. J.* **103**, 852-862 (1967).

11. T. Maack: Renal clearance and isolated kidney perfusion techniques. *Kidney Int.* **30**, 142-151 (1986).

12. J. Peterson, J. Kitaji, W.C. Duckworth, and R. Rabkin: Fate of [^{125}I]insulin removed from the peritubular circulation of isolated perfused rat kidney. *Am. J. Physiol.* **243**, F126-F132 (1982).

13. B. Draznin, M. Trowbridge, and L. Ferguson: Quantitative studies of the rate of insulin internalization in isolated rat hepatocytes. *Biochem. J.* **218**, 307-312 (1984).

14. A.E. Gibson, R.J. Noel, J.T. Herlihy, and W.F. Ward: Phenylarsine oxide inhibition of endocytosis: Effects on asialofetuin internalization. *Am. J. Physiol.* **257**, C182-C184 (1989).

15. T. Terasaki, K. Hirai, H. Sato, Y.S. Kang, and A. Tsuji: Absorptive-mediated endocytosis of a dynorphin-like analgesic peptide, E-2078, into the blood-brain barrier. *J. Pharmacol. Exp. Ther.* **251**, 351-357 (1989).

16. H. Sato, A. Tsuji, K. Hirai, and Y.S. Kang: Application of HPLC in disposition study on A14-^{125}I-labeled insulin in mice. *Diabetes* **39**, 563-569 (1990).

17. B. Sactor, I.L. Rosenbloom, C.T. Liang, and L. Cheng: . *J. Membrane Biol.* **60**, 63-71 (1981).

18. H. Sato, K. Takeda, T. Terasaki, and A. Tsuji: Specific binding of β-endorphin to the isolated renal basolateral membranes in vitro. *Chem. Pharm. Bull.* **38**, 3395-3399 (1990).

19. R. Rabkin and A.E. Kitabchi: Duckworth. *J. Clin. Invest..62* **169.175**, 1978-Factors influencing the handling of insulin by the isolated rat kidney (20).

C.. F.G. Hamel, J. Liepnieks, D. Peavy, B. Frank, and R. Rabkin: Insulin degradation products from perfused rat kidney. *Am. J. Physiol.* **256**, E208-E214 (1989).

21. O. Sonne: Receptor-mediated degradation of insulin in isolated rat adipocytes. Formation of a degradation products slightly smaller than insulin. *Biochim. Biophys. Acta* **927**, 106-111 (1987).

22. F.G. Hamel, E.D. Peavy, M.P. Ryan, and W.C. Duckworth: HPLC analysis of insulin degradation products from isolated hepatocytes. *Diabetes* **36**, 702-708 (1987).

23. H.S. Wiley and D.D. Cunningham: The endocytotic rate constant. A cellular parameter for quantitating receptor-mediated endocytosis. *J. Biol. Chem.* **25**, 4222-4229 (1982).

24. J.R. Levy and J.M. Olefsky: The trafficking and processing of insulin and insulin receptors in cultured rat hepatocytes. *Endocrinology* **121**, 2075-2086 (1987).

25. M.L. Standaert and R.J. Pollet: Equilibrium model for insulin-induced receptor down-regulation. Regulation of insulin receptors in differentiated BC3H-1 myocytes. *J. Biol. Chem.* **259**, 2346-2354 (1984).

26. G.R. Wilkinson and D.G. Shand: Commentary. A physiological approach to hepatic drug clearance. *Clin. Pharm. Ther.* **18**, 377-390 (1975).

27. A. Tsuji, T. Yoshikawa, K. Nishide, H. Minami, M. Kimura, E. Nakashima, T. Terasaki, E. Miyamoto, C.H. Nightingale, and T. Yamana: Physiologically based pharmacokinetic model for β-lactam

antibiotics I: tissue distribution and elimination in rats. *J. Pharm. Sci.* **72**, 1239-1252 (1983).

28. H. Sato, Y. Sugiyama, Y. Sawada, T. Iga, and M. Hanano: Binding of radioiodinated human β-endorphin to serum proteins from rats and humans, determined by several methods. *Life Sci.* **37**, 1309-1318 (1985).

29. R. Rabkin, T.I. Gottheiner, and T. Tsao: Metabolic characteristics of renal insulin uptake. *Diabetes* **30**, 929-934 (1981).

30. D.L. Maude, D.G. Handelsman, M. Babu, and E. Gordon: Handling of insulin by the isolated perfused rat kidney. *Am. J. Physiol.* **240**, F288-F294 (1981).

31. E. Schlatter, H.J. Schurek, and R. Zick: Renal handling of homologous and heterologous insulin in the isolated perfused rat kidney. *Pflugers Archiv.* **393**, 227-231 (1982).

32. J. Gliemann, O. Sonne, S. Linde, and B. Hansen: Biological potency and binding affinity of monoiodoinsulin with iodine in tyrosine A14 or tyrosine A19. *Biochem. Biophys. Res. Com.* **87**, 1183-1190 (1979).

33. B.H. Frank, D.E. Peavy, C.S. Hooker, and W.C. Duckworth: Receptor binding properties of monoiodotyrosyl insulin isomers purified chromatography. *Diabetes* **32**, 705-711 (1983).

34. C. Whiteside and M. Silverman: Determination of postglomerular permselectivity to neutral dextrans in the dog. *Am. J. Physiol.* **245**, F496-F505 (1983).

35. P. De Meyts, R. Bianco, and J. Roth: Site-site interactions among insulin receptors. Characterization of the negative cooperativity. *J. Biol. Chem.* **251**, 1877-1888 (1976).

36. D.K. Reed, C. Newton, M. Fraga, K. Glastad, A. Bagheri, S. Harris, and B.C. Reed: An analysis of the relationship between the cellular distribution and the rate of turnover for the separate classes of unoccupied, noncovalently occupied, and covalently occupied insulin receptor. *J. Biol. Chem.* **264**, 12673-12679 (1989).

37. E. Maratos-Flier, C.Y. Kao, E.M. Verdin, and G.L. King: Receptor-mediated vectorial transcytosis of epidermal growth factor by Madin-Darby canine kidney cells. *J. Cell Biol.* **105**, 1595-1601 (1987).

38. J. Herrman, R.E. Simmons, B.H. Frank, and R. Rabkin: Differences in renal metabolism of insulin and cytochrome *c*. *Am. J. Physiol.* **254**, E414-E428 (1988).

39. J.T. Nielsen and E.I. Christensen: Basolateral endocytosis of protein in isolated perfused proximal tubules. *Kidney Int.* **27**, 37-45 (1985).

TABLE 1.

Characteristics of the filtering and nonfiltering perfused rat kidneys[a]

Characteristics	Filtering	Nonfiltering
Kidney weight (g)	1.28 ± 0.04 (9)	1.39 ± 0.02 (18)
Hematocrit (%)	11.7 ± 0.2 (9)	11.6 ± 0.2 (18)
Perfusion pressure (mmHg)	102.5 ± 0.2 (9)	65.4 ± 0.9 (6)
Flow rate (ml/min)[b]	4.38 ± 0.17 (9)	3.98 ± 0.36 (6)
Urine flow (µl/min)	17.2 ± 1.0 (9)	N.D.[c]
GFR (ml/min/g kidney)[b]	0.428 ± 0.019 (3)	0.0518 ± 0.0073 (3)
Insulin clearance (ml/min/g kidney)[b]	0.480 ± 0.021 (3)	0.133 ± 0.023*(3)

[a] The data are expressed as the means ± SEM. The numbers in parentheses represent the number of rats used for the determination of the characteristics of the perfused kidneys.

[b] Expressed in terms of the erythrocyte-free perfusate. The GFR and insulin clearance were calculated by Eqn. (1).

[c] Not determined.

* $P < 0.01$, significantly different from the filtering kidney by Student's *t*-test.

FIGURE LEGENDS

Fig. 1. *HPLC chromatograms of A_{14}-^{125}I-insulin in the perfusate before (panel A) and after (panel B) 60-min perfusion of the nonfiltering rat kidneys.*

Open circles represent ^{125}I-radioactivity (cpm) in 0.8-ml fractions eluting from μ-Bondapak C_{18} column (30 cm x 3.9 mm i.d., Waters) with the acetonitrile gradient shown by a broken line. Flow rate was set at 1 ml/min.

Fig. 2. *HPLC chromatograms of acid-extractable (panel A) and acid-resistant (panel B) A_{14}-^{125}I-insulin in the perfusate after 60-min perfusion of the nonfiltering rat kidneys.*

The HPLC conditions used are the same as in Fig. 1.

Fig. 3. *Time dependence of acid-extractable (○) and acid-resistant (●) A_{14}-^{125}I-insulin as well as acid-resistant degradation products of A_{14}-^{125}I-insulin (▲) in the nonfiltering rat kidneys, measured separately by the acid-wash technique and TCA-precipitation (for details see* Materials and Methods *section).*

Fig. 4. *Effects of phenylarsine oxide (250 μM) on the acid-extractable and acid-resistant A_{14}-^{125}I-insulin after 60-min perfusion of the nonfiltering kidneys.*

Since phenylarsine oxide was dissolved in DMSO and used after 1000-dilution, the same concentration (0.01%) of DMSO was also included in the perfusion media in control experiments. * Significantly different from control at $p < 0.01$ by Student's *t*-test.

Fig. 5. *Effects of unlabeled insulin (1 μM) on the acid-extractable and acid-resistant A_{14}-^{125}I-insulin after 60-min perfusion of the nonfiltering kidneys.*

* Significantly different from control at $p < 0.01$ by Student's *t*-test.

Fig. 1

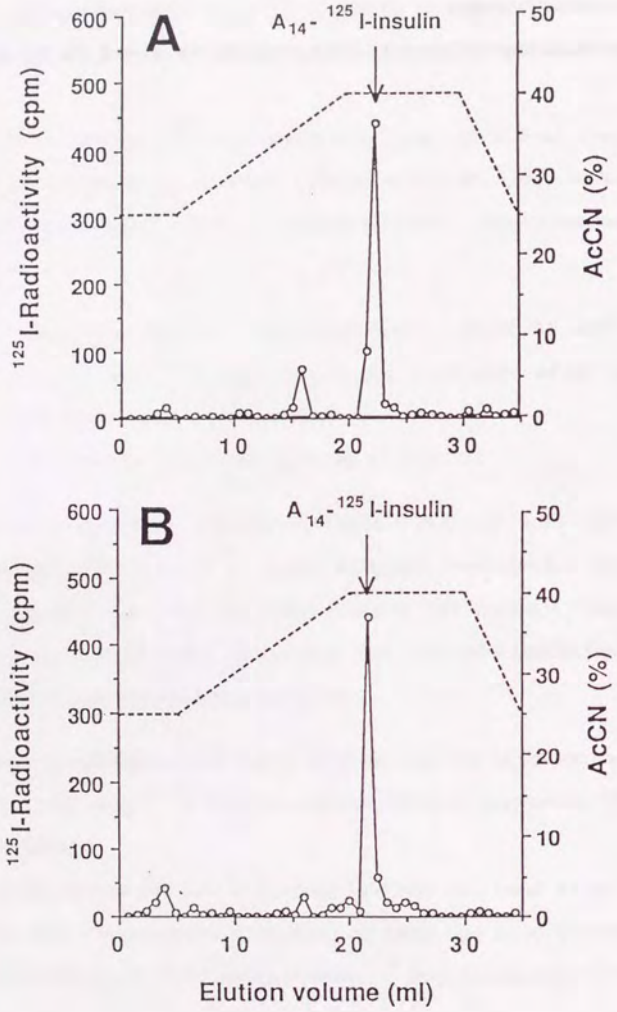
A
B
A_{14}- ^{125}I-insulin
^{125}I-Radioactivity (cpm)
AcCN (%)
Elution volume (ml)

Fig. 2

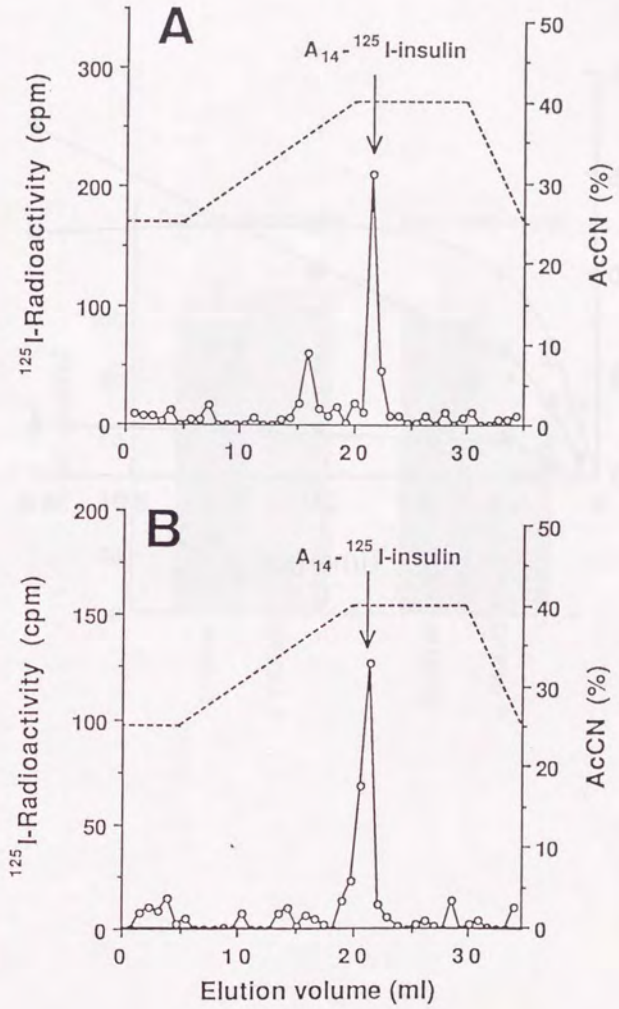
A
B
A_{14}- ^{125}I-insulin
^{125}I-Radioactivity (cpm)
AcCN (%)
Elution volume (ml)

Fig. 3

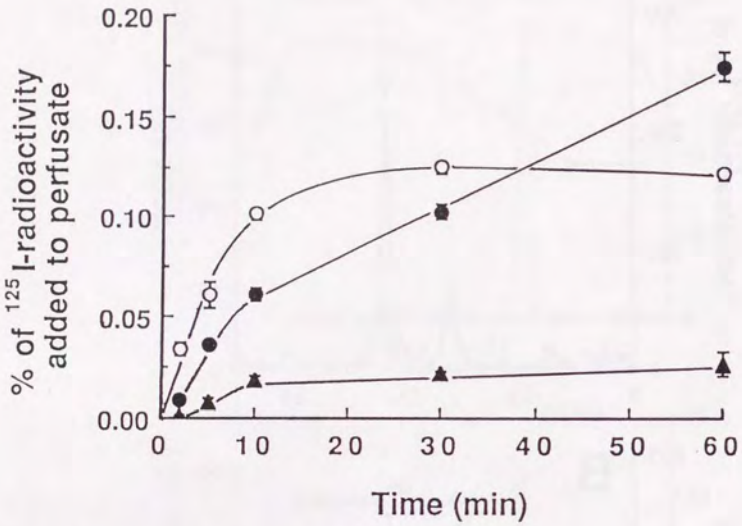
0.20
0.15
0.10
0.05
0.00
% of 125 I-radioactivity added to perfusate
0
10
20
30
40
50
60
Time (min)

Fig. 4

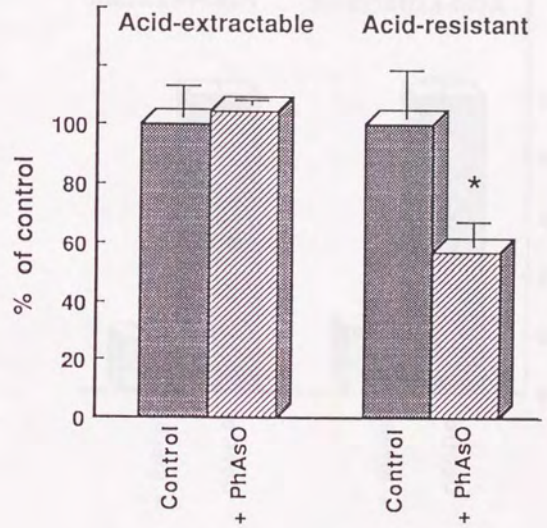
Acid-extractable
Acid-resistant
% of control
100
80
60
40
20
0
*
Control
+ PhAsO
Control
+ PhAsO

Fig. 5

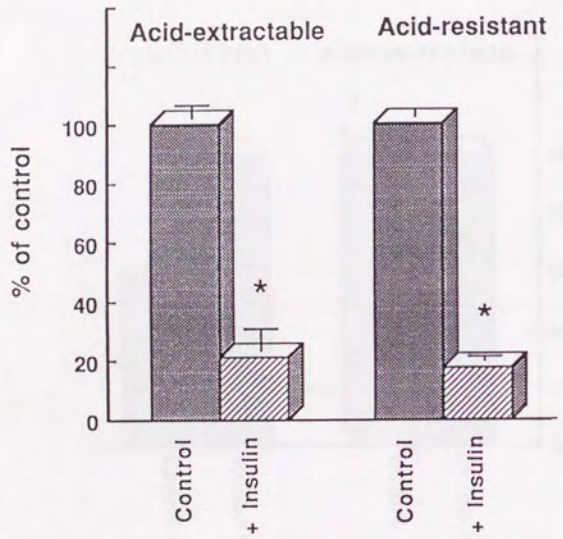
Acid-extractable
Acid-resistant
% of control
100
80
60
40
20
0
*
*
Control
+ Insulin
Control
+ Insulin